# Climate, Sea Level and Tectonic Controls on Sediment Discharge from the Sepik River, Papua New Guinea during the Mid- to Late Pleistocene

- 3 Aiello, I.W.<sup>1</sup>, Bova, S.C.<sup>2</sup>, Holbourn, A.E.<sup>3</sup>, Kulhanek, D.K.<sup>4</sup>, Ravelo, A.C.<sup>5</sup>, and Rosenthal, Y.<sup>2</sup>
- <sup>1</sup> Moss Landing Marine Laboratories, 8272 Moss Landing Rd., Moss Landing, CA 95039
- <sup>2</sup>Department of Marine and Coastal Sciences Rutgers, 71 Dudley Road, New Brunswick NJ 8521
- <sup>3</sup>Institute of Geosciences, Christian-Albrechts-Universität zu Kiel, Ludewig-Meyn-Strasse 14, Kiel
- 7 24118, Germany

1

2

- <sup>4</sup>International Ocean Discovery Program, 1000 Discovery Drive, College Station, TX 77845, USA
- Ocean Sciences Department, University of California, Santa Cruz, 1156 High Street, Santa Cruz CA
   95064

# Abstract

11

12

13

14

15

16

17

18

19

20

21

22

23

Amongst the rivers draining the mountainous islands of the Indonesian Archipelago, the Sepik River of Papua New Guinea is the largest contributor of solute and particulate material to the world ocean. Sites U1484 and U1485, drilled during International Ocean Discovery Program (IODP) Expedition 363 provide a continuous, ~555 kyr long, high-resolution record of mainly siliciclastic slope sedimentation on the northern continental margin of PNG, just offshore the mouth of the Sepik River. Sedimentological analysis, based on a combination of smear slide petrography, particle size analysis, high-resolution physical properties track data and visual core description, offers an unprecedented opportunity to investigate the evolution of this major tropical river throughout changing climate and sea-level conditions during the mid- to late Pleistocene. The Sites U1484 and U1485 sediment records exhibit a dramatic lithologic change at ~ 370 ka: the oldest deposits are dominated by pelagic mud, suggesting that the coarser-grained terrigenous discharge from rivers draining the New Guinea Highlands (including a "proto" Sepik River) was captured before reaching the ocean, when the Sepik River basin was an

epicontinental sea. The occurrence of coarser-grained, mass-gravity (mainly hybrid) flows after ~370 ka suggests that the epicontinental sea became a more restricted, shallow-water to nonmarine basin, probably due to both basin infilling and the uplift of local coastal ranges. During the last three glacial-interglacial cycles (~300 kyr), this shallow inland basin was strongly affected by global variations in sea level: during sea level lowstands, the Sepik River cut into older sediments and discharged further offshore onto the shallow continental margins, promoting mass-gravity flows. Pelagic mud deposition on the continental margin during the most extreme highstands following deglaciations suggests a return to shallow marine conditions in the Sepik Basin and repositioning of the river mouth further inland, away from the shelf and from the location of the IODP sites. This also indicates that variations in terrigenous fluxes during these extreme highstands were not solely controlled by the intensity of the hydrological cycle and that global sea level variations also influenced sediment deposition. The sequence is interrupted by several massive grain flow deposits, occurring diachronously at Sites U1484 and U1485 and related to a period of intensified tectonic activity between ~280 ka and ~140 ka. The sedimentologic characteristics of these mass-gravity deposits and their lack of correlation between sites are interpreted as resulting from channelized flows along margin-parallel, fault-controlled channels caused by local and regional failures of the continental margins including the area of the Yalingi Canyon, ~50 km north of the sites, where large tsunamigenic events have also occurred in recent years. Time series analyses of magnetic susceptibility and natural gamma radiation (proxies for %sand and %clay content, respectively) indicate that river discharge fluxes were modulated at orbital frequencies (including obliquity-scale cycles), which suggests that precipitation and river discharge were not only linked to precessionally driven shifts in the mean position of the Intertropical Convergence Zone, but also to high-latitude climate change.

24

25

26

27

28

29

30

31

32

33

34

35

36

37

38

39

40

41

42

43

44

45

46

47

**Keywords:** Papua New Guinea; Sepik River; IODP; mass-gravity deposits; successor basin; tropical rivers

#### 1 Introduction

48

49

50

51

52

53

54

55

56

57

58

59

60

61

62

63

64

65

66

67

68

69

70

71

# 1.1 Importance of Sediment Discharge from Tropical Rivers

Rivers are Earth's dominant circulatory systems and are responsible for transferring water, solute, and particulate material from highland elevations to the deep ocean, largely in a serial path (Nittrouer et al., 2017; Gaillardet et al., 1999; Viers et al., 2009). More than 70% of the sediment entering the world ocean comes from rivers draining southeast Asia and the relatively small rivers of the Indonesian Archipelago islands (collectively known as the 'Maritime Continent') owing to the combination of warmth, high rainfall, lithology, and relief (Milliman and Meade, 1983). The Indonesian Archipelago is under the direct influence of the Intertropical Convergence Zone (ITCZ), where deep convection gives rise to the heaviest rain belt on Earth. Small rivers generally discharge much greater loads relative to their drainage basin areas than large rivers because of the lesser storage capacity and greater exposure to episodic events such as landslides (Milliman and Syvitski, 1992). Four of the world's five largest rivers, in terms of rates of chemical weathering and consequent CO<sub>2</sub> consumption rate per unit area, drain basins on the island of New Guinea (Gaillardet et al., 1999). These rivers discharge approximately  $1.7 \Pi 10^9$  tons of sediment to the ocean annually (Milliman, 1995), which is about the same as all the rivers draining North America combined (Milliman and Meade, 1983). Rivers draining the Indonesian Archipelago islands could have contributed in multiple ways to climate change during the late Neogene. The growth of the Maritime Continent during the Pliocene (~60% of the islands' land area formed over the past 5 Myr; Molnar and Cronin, 2015) could have directly contributed to part of the atmospheric  $pCO_2$  drop since 5 Ma due to the resulting increase in silicate weathering. Island formation could have also enhanced rainfall over the region, which in turn strengthened the Walker Circulation, contributing to cooling of eastern equatorial sea-surface temperatures (SSTs) in the Pacific and, through teleconnections, enabling the inception of the Laurentide Ice Sheets (Molnar and Cronin, 2015). Sediments derived from the Indonesian Archipelago could be a

major source of reactive Fe (a major limitation to phytoplankton production in the open ocean; Martin, 1992) associated with particulate aluminum transported to the eastern equatorial Pacific by way of the Equatorial Undercurrent (EUC; Figure 1), thus playing an important role in the biological pump (Milliman et al., 1999). Winckler et al. (2016) suggested that the supply of micronutrients from the Southern Ocean, as well as from the weathering of volcanic rocks in Papua New Guinea (PNG; Figure 1), could have had a much larger role than atmospheric dust in fueling productivity in the high-nutrient, low-chlorophyll region of the Eastern Equatorial Pacific during the late Pleistocene.

A series of important transitions occurs before and after a fluvial system reaches sea level. These transitions determine what portion of the sediment load accumulates in the alluvial plains and in delta systems, and what portion accumulates nearshore and/or is transported to the deep sea. The morphology of the continental margin has a fundamental role in determining the fate of fluvial sediments once they enter the oceans. In PNG, the sediments discharged on the southern side of the island (e.g. Fly River; Figure 1) accumulate onto broad shallow shelves and only a small portion escapes to the deep ocean (Milliman et al., 1999). In contrast, the continental shelf northwest of the Sepik River mouth is less than 1-2 km wide, and most sediment discharged through the delta bypasses the shelf, escaping seaward via the Sepik Canyon (Kineke et al., 2000; Kuehl et al., 2004). The Sepik River deltaic plain is a relatively young feature. Globally, many deltaic plains started forming only after ~8,000 years ago, when the rate of sea level rise slowed (Stanley and Warne, 1994). For instance, in the modern Mekong Delta, sea level regression along the delta front began about 4,800 years ago and coincided with the local slowdown of sea level rise that allowed buildup of a subaerial delta (Bird et al., 2010; Liu et al., 2017). According to Chappell (1993), the Sepik River delta started forming even later than the Mekong delta, and rapid delta progradation did not begin when Holocene sea level first stabilized, but only ~3000 years ago, probably because the rivers could not feed the deltaic plain until the inland portion, still occupied by a shallow sea, was sufficiently filled with sediment.

#### 1.2 Study Rationale

72

73

74

75

76

77

78

79

80

81

82

83

84

85

86

87

88

89

90

91

92

93

94

95

96

A number of studies have focused on high-resolution, deep-sea sediment records that capture the history of sediment discharge from tropical rivers to the deep ocean during the Pleistocene (e.g. Clift, 2006; Clift et al., 2008; Zhang et al., 2016; Liu et al., 2017; Wan et al., 2017), but the history of river discharge from tropical mountainous islands of the Indonesian Archipelago, including PNG, has received less attention. Downcore variations of the element Ti from high-resolution X-Ray Fluorescence (XRF) analyses of piston core MD05-2920 (collected near Manus Island; Figure 1), were interpreted by Tachikawa et al. (2011) as indicative of terrigenous fluxes from the Sepik River. Terrigenous inputs are detected over the full length of the core, which indicates river discharge persisted for at least the last 400 kyr. Time series analysis of Core MD05-2920 XRF data also revealed that river discharge was controlled by precipitation variability at the precession band, suggesting that the hydrological cycle of the Western Pacific Warm Pool was closely associated with the East Asian Monsoon (Tachikawa et al., 2011). This interpretation is consistent with previous proxy studies (Wang et al., 2008; Cruz et al., 2005) supporting the hypothesis that both the boreal and austral summer monsoons responded to precessional forcing (Beaufort et al., 2010). Analysis of foraminiferal rare earth elements (REE)s in Core MD05-2925 (Liu et al., 2015) just offshore the east coast of southern PNG showed that for the last ~280 kyr, terrigenous fluxes to the continental margins varied at both the obliquity and precessional scale. Modeling simulation supports the interpretation that during conditions of high-obliquity the mean position of the ITCZ moved further south than the latitudes of PNG while during conditions of low-obliquity and high-precession the ITCZ was further to the north and, as a consequence, during those times PNG experienced heavy rainfall (Liu et al., 2015). High-resolution records of river discharge variability from large mountainous islands of the

97

98

99

100

101

102

103

104

105

106

107

108

109

110

111

112

113

114

115

116

117

118

119

120

121

High-resolution records of river discharge variability from large mountainous islands of the Indonesian Archipelago, such as that related to the Sepik River of PNG, can offer important clues to the dynamics of the ITCZ during the Pleistocene and can help determine whether the Western Pacific region was a potential source of micronutrients to the equatorial Pacific upwelling system. However, variations in terrigenous fluxes to the continental margins are not always a simple function of hydrological cycle

intensity. Multiple factors, several of which are not directly related to climate, can affect the residence time and pathways that river sediments take from their source areas to the continental margins. One factor is the presence of inner basin(s) that trap sediments before they reach the shore. Other factors include the location of the river mouth in relation to seafloor features such as canyon heads that might funnel the coarser sediment fraction directly to the slope or the redistribution of sediments by coastal currents. The potential for sediments discharged by river floods to be preserved in continental margin sedimentary records is also dependent on the extent of post-depositional processes such as mass-gravity flows, which are common in tectonically active regions such as PNG.

The geological units exposed in the Bewani, Alexander and Torricelli Ranges (also referred to as the Northern Ranges of PNG; Figure 1) and the sediments recovered by exploration wells in the Sepik Valley indicate that Holocene sedimentation represents the latest stage of a successor basin that developed in the Miocene and has since been affected by tectonic movements and sea-level changes during glacial-interglacial cycles (Dow, 1977; Chappell, 1993). Because of local tectonic activity, with uplift rates of the Northern Ranges as high as 8 m/kyr (e.g. Torricelli Range; Gill, 1967 reported in Swalding et al., 1989), the geography of the coastal region and the morphology of the continental margins have changed dramatically throughout the Pleistocene. As suggested by U-series measurements of aragonitic coral reef outcrops exposed in the region, the Sepik region was an inland sea at least until ~296 ka +33/-26 kyr (Swalding et al., 1989). The sea was barred by young emerging coastal ranges first to the south (Adalbert Range) and then to the north (Northern Ranges; Figure 1; Chappell, 1993). In the presence of a marine embayment, the Sepik and Ramu Rivers were probably discharging much further inland compared to the location of today's river mouths and the storage capacity of the basin was much larger than that of the Sepik Valley today.

The sediments recovered by International Ocean Discovery Program (IODP) Expedition 363 at Sites U1484 (1031 m water depth and cored to a total depth of ~224 m below seafloor [mbsf]) and U1485 (1145 m water depth, core to ~300 mbsf), located north of the mouth of the Sepik River (Table 1; Figure

1), are mainly siliciclastic and composed of silt, clay, and subordinately sand, whereas biogenic and authigenic components such as calcareous nannofossils, foraminifers and sulfides generally occur in trace amounts. Fine-grained siliciclastic intervals alternate with discrete layers of coarser, sand- and silt-size sediment. Several of the coarser-grained layers show sedimentary structures indicating deposition from density flows and include shell debris and plant material, suggesting multiple steps including a subaerial and nearshore phase, before their final deposition on the continental margin (Rosenthal et al., 2018). At Site U1485, which has the longest stratigraphic record, the middle Pleistocene is dominated by fine-grained hemipelagic and pelagic sediments (Subunit IB of Rosenthal et al., 2018), whereas the middle to late Pleistocene portion includes coarser-grained beds and massive, meter-thick sand-rich layers (Subunit IA; Rosenthal et al., 2018). This continuous sediment record offers the opportunity to reconstruct for the first time the river discharge from a major tropical mountainous island within the Indonesian Archipelago. In particular, we aim to constrain the onset of sediment discharge from the Sepik River to the world ocean and to reconstruct how terrestrial topography, river discharge and continental margin sedimentation evolved in relation to changes in climate and sea level during glacial-interglacial cycles and to the dynamic tectonic regime characterizing the PNG region.

#### 2 Regional Setting

#### 2.1 Tectonic and Geologic settings

Here we synthesize some of the geological and tectonic reconstructions for the PNG region from the last several decades that are relevant to this study (e.g. Dow, 1977; Jaques and Robinson 1977; Hamilton, 1979; Abbott et al. 1994; Crowhurst et al. 1996; Hall 2002; Hill and Hall 2003; Cloos et al., 2005; Woodhead et al. 2010; Baldwin et al., 2012; Davies 2012; Holm and Richards, 2013). The main tectonic process responsible for the formation of the Indonesian Archipelago island arcs is the northward movement of Australia towards the Eurasian Plate from higher southern latitudes into the equatorial region and the resulting subduction that forms the Java Trench and Timor Trough. The tectonic setting of

the southwest Pacific Ocean and PNG is more complex. Oblique convergence between the Australian and Pacific plates resulted in the formation of several microplates and the development of oblique spreading centers between the late Eocene and early Miocene. Oblique convergence is accommodated partly by leftlateral strike-slip motion on E-W fault systems and partly by transpressional and strike-slip faulting in the PNG fold belt (Figure 1). In northwestern New Guinea, the Australian and Pacific Plates converge along the New Guinea Trench. Offshore, the motion between the Bismarck Plate and the Pacific Plate to the north is associated with the Bismarck Sea Seismic Lineation (BSSL) defined primarily by earthquake epicenter locations and characterized by left-lateral transform faults and associated step-over rifts (Taylor 1979; Cooper and Taylor, 1987; Figure 1). This trend continues on land as a series of faults that cut westward through the Torricelli and Bewani Ranges (Ripper et al., 1980). Magnetic anomalies in the Bismarck Sea indicate rapid asymmetric spreading since 3.5 Ma (Taylor 1979). The South Bismarck Plate is currently rotating clockwise at a rate of 8°/Ma relative to Australia, whereas the west-northwest motion of the North Bismarck Plate is similar to that of the Pacific plate (Tregoning et al. 1999; Wallace et al. 2004). In the eastern Bismarck Sea, the East Manus spreading center separates the North and South Bismarck Plates (Martinez and Taylor 1996), whereas in the western Bismarck Sea, the boundary becomes the BSSL (Baldwin et al., 2012).

The hinterland region (New Guinea Highlands) is made up of terranes that have accreted to the Australian craton in a succession of collisions that started in the Late Cretaceous. The terranes include fragments of Paleozoic craton, ophiolites, a variety of metamorphic rocks, dioritic/granodioritic intrusives, island arc volcanic rocks and associated sediments, and oceanic crustal rocks. They are partly unconformably covered by early to middle Miocene and younger age sediment that can be as much as 10 km thick (Davies, 2012). Previous research has suggested that the mountain ranges that extend from the Huon peninsula toward the northwestern margin of PNG consist of accreted island arc(s) (e.g. the Melanesian Arc of Crowhurst et al. 1996) unconformably overlain by Miocene–Pliocene limestone (Jaques, 1977). The collision of these terranes is interpreted as having been the result of the closure of the

Solomon Sea at the New Britain trench, owing to subduction-driven convergence between the Australian and South Bismarck plates (e.g. Abbott et al., 1994; Hill and Raza, 1999; Weiler and Coe, 2000). In northern PNG, the accreted arc terranes include the Cyclops Mountains, the Bewani-Torricelli Ranges, the Amanab block and the Finisterre Ranges (Figure 1). The youngest and most significant of these collisions, initiated at ~3.7 Ma, resulted in the accretion of the Adelbert and Finisterre Terranes, with the convergence being presently accommodated by activity along the Ramu-Markham Thrust Fault (e.g. Cooper and Taylor 1987; Abbott et al. 1994; Pegler et al. 1995; Figure 1). The inferred timing of plate coupling at ~3.7 Ma is coincident with the earliest breakup and opening of the New Britain back-arc and the formation of the North and South Bismarck microplates (Taylor 1979; Abbott et al. 1994).

Major faulting and folding accompanied by widespread igneous activity began between the latest Miocene and the beginning of the Pliocene and resulted in the uplift of most of the mountains in PNG today. By the late Pliocene most of the present highlands were emergent, and sedimentation was mainly restricted to the Sepik Embayment, a shallow water gulf that covered approximately the same location of today's Sepik River valley. In Dowe's (1977) paleogeographic reconstructions, during the Pliocene the Sepik Embayment was connected to the Gulf of Papua through a narrow inlet along the Ramu-Markhan Fault Zone (the Aure Trough).

#### 2.2 Climate and Oceanography

The climatology of PNG is strongly influenced by the seasonal migration of the ITCZ, with enhanced precipitation during boreal winter and decreased precipitation during El Niño events (Tachikawa et al, 2011). Monsoon winds control the surface hydrography of the region, such that the New Guinea Coastal Current (NGCC) flows north-westward over Sites U1484 and U1485 during the boreal summer southeasterly monsoon (Cresswell, 2000; Kuroda, 2000; Figure 1). These currents distribute sediments originating from the Sepik and Ramu River mouths and other tributaries along the coast. The NGCC reverses during the boreal winter northwesterly monsoon (Kuroda, 2000), and the surface sediment plume from the Sepik River is observed to meander out across the Bismarck Sea. A subsurface

current found at depths below 200 m, the New Guinea Coastal Undercurrent (NGCUC; Figure 1), flows toward the west throughout the year, and strengthens during the southeast monsoon in the boreal summer (Fine et al., 1994; Cresswell, 2000; Kuroda, 2000).

The Sepik River watershed extends approximately east-west from the east coast of PNG to the hinterland and to the border between the Independent State of Papua New Guinea and the Republic of Indonesia. The watershed includes the New Guinea Highlands to the south and the coastal Bewani-Torricelli Ranges to the north (Figure 1). The Yuat River, the largest tributary of the Sepik River, extends the watershed to the south, to the foothills of the New Guinea Western Highlands. The Ramu River flows subparallel to the Yuat River, and the watershed extends further south between the coastal Finisterre Range and the Southern Highlands (Figure 1). The present day Sepik River mouth intersects a submarine canyon that transverses the narrow (~5 km) continental shelf. Reconnaissance studies off the Sepik (Kineke et al., 2000) and <sup>210</sup>Pb geochronology of Kasten cores from the continental margin area adjacent to the river mouth (Kuehl et al., 2004) suggest that a substantial portion of the riverine sediment (up to 93%) could bypass the shelf and upper slope and be transported seaward in the canyon, where it escapes offshore via gravity flows. Salinity and suspended sediment distributions along the canyon axis from the river mouth to the coastal ocean suggest that sediment is dispersed via a plume with both hypopycnal and hyperpycnal components.

#### Materials and Methods

# 3.1 Age Models: $^{14}C$ and $\delta^{18}O$

The age model for Site U1485 (Supplementary Table 1A and Figure S1) is based on shipboard biostratigraphy (Rosenthal et al., 2018) and is further constrained by four Accelerator Mass Spectrometry  $^{14}$ C dates obtained from the surface-dwelling planktonic foraminifer *Globigerinoides ruber*, and by correlation between a preliminary low resolution  $\delta^{18}$ O planktonic foraminifer record for this site and the reference benthic foraminifer isotope stack LR04 (Lisiecki and Raymo, 2005). The resulting age model

suggests an average linear sedimentation rate of about 70 cm/kyr. The age model for Site U1484, based on correlation of a preliminary low resolution planktonic foraminifer  $\delta^{18}$ O record to the reference benthic LR04 isotope stack (Lisiecki and Raymo, 2005; Supplementary Table 1B and Figure S1), suggests an average linear sedimentation rate of about 90 cm/kyr.

#### 3.2 Laser Particle Size Analysis (LPSA)

245

246

247

248

249

250

251

252

253

254

255

256

257

258

259

260

261

262

263

264

265

266

267

268

269

Low resolution samples (644 in total) were collected at approximately regular intervals of 1 sample per section (1 section is ~1.5 m) at both Sites U1484 and U1485 (Supplementary Data). Additional higher resolution samples focusing on the coarser-grained intervals (312 samples) were collected from Site U1485 (Supplementary Data). To investigate the distribution of grain sizes the samples were analyzed using a Laser Particle Sizer Analyzer (LPSA). We used a Beckman-Coulter LS 13 320 (the instrument uses a 5 mW laser diode with a wavelength of 750 nm). This instrument analyzes small (~0.5 to 2.0 g) masses of unconsolidated sediment and combines conventional laser beam diffraction with polarized intensity differential scattering allowing highly resolved grain size measurements (126 logarithmically spaced channels between 0.04 µm and 2.00 mm; Beckman Coulter Inc., 2003). Laser diffraction particlesize measurement is based on the Fraunhofer and Mie theory of light scattering, whereby spherical particles of a given size diffract light at a specific angle, with the angle increasing with decreasing particle size (Singer et al., 1988). Geometric statistics were applied to the values obtained by the logarithmically spaced size channels of the particle analyzer using the method of moments, since Expedition 363 samples tend to have log-normal grain size distributions in the 0.04 µm to 2 mm spectrum. This analytical method has successfully been used on core sediments of mixed biogenic and siliciclastic composition (Aiello and Ravelo, 2012) and siliciclastic sediments (Filidani et al., 2018). The sample is diluted in a 1.2 L aqueous module filled with deionized water equipped with a pump unit running at 100% power. The sample is added to the module until optimal obscuration conditions are reached, with the latter determined automatically by the instrument. Previous experiments have suggested that in sand samples mixed with clay and silt, standard obscuration conditions might not capture the full extent of the particle size

distribution (Filidani et al., 2018). With increasing obscuration conditions beyond the standard value indicated by the instrument, a larger range of particles is measured until an optimal concentration is reached. Accordingly, the obscuration value used was approximately twice the standard value. Preliminary tests indicated that disaggregation of the sample (e.g. using sonication) prior to the analysis was unnecessary and that the energy of the water controlled by the pump was sufficient to ensure complete disaggregation. The tests also showed a lack of flocculation; thus, dispersants (e.g. Calgon) were not used. One advantage of using LPSA include the small sample size required for the analysis. A disadvantage is the limit of the maximum measurable grain size (2000 µm), and previous studies have shown that the analysis of the distribution of the fine-grained fraction (clay and fine silt) is less accurate in LPSA compared to settling methods (e.g. Konert and Vandenberghe, 1997). The platy shape of clay affects the light scattering such that the instrument returns a larger size, potentially resulting in an underestimation of the clay fraction. However, McCave et al. (2006) demonstrated that differences in estimates of the mean and relative percentage of the silt and finer grain-size fraction from LPSA versus settling methods were negligible.

#### 4 Results

#### 4.1 Sedimentation Rates

The sedimentary record recovered at Site U1484 covers a shorter interval (~305 ka) and the average sedimentation rate is higher (90 cm/kyr) than at Site U1485 (~555 ka and 67 cm/kyr, respectively; Figure 2; Table 1). Sedimentation rates at the two sites are comparable only over the last ~30 kyr. The highest rates (~1 m/kyr) occurred between ~245 and 285 ka at Site U1485 and between ~140 and 200 ka at Site U1484, when homogenous, massive sand layers were deposited (asterisks in Figure 2; Figures 3A and 3B). The older part of the record (>~370 ka) is dominated by fine-grained sedimentation (green bar in Figures 2 and 3B) including an interval of nannofossil ooze between ~400 and 435 ka. This interval exhibits the lowest sedimentation rates at Site U1485 (0.22 m/kyr; purple bar in Figures 2 and 3B).

### 4.2 Sediment Composition

The sediment recovered at Sites U1484 and U1485 consists mainly of fine-grained siliciclastics as shown by the relative proportions of sand, silt, and clay obtained from the LPSA analyses and plotted using the classification scheme for siliciclastic sediments of Folk (1954, 1974; Figure 4A). Using Folk's (1954) original classification, the samples fall into five separate fields: mud, silt, silty sand, sandy mud and sandy silt (hereafter indicated in italics): combined, *mud* and *silt* include the highest proportion of the sediments (~89%), ~7% are *sandy silt*, and ~4% are in the coarsest field *silty sand* (Figure 4A). Although sedimentary layers with different textures alternate at meter- and sub-meter scales, one of the three sediment textures identified generally dominates over several contiguous cores (on average 1 core is ~9.5 m or ~7-10 kyr).

Sediments with dominant *mud* and *silt* textures are concentrated in six distinct intervals (outlined by green bands in Figures 2, 3A and 3B; also listed in Table 2). The youngest of these intervals includes the last ~11 kyr of sedimentation (Figure 5A). *Mud* and *silt* is the dominant sediment texture of the oldest, >~370 ka portion of the record at Site U1485, and it includes an ~50 kyr-long interval of predominantly nannofossil ooze with the slowest sedimentation rates for this site (purple band in Figures 2 and 3B; Figure 5B). The sediments with the coarsest, *silty sand* texture (asterisks in Figure 2; brown bands in Figure 3; Figure 5C) occur as massive layers that are diachronous between the two sites. The youngest of these layers at Site U1484 (between ~135 and ~177 ka) includes massive, homogenous sand, which was saturated in some intervals when recovered and showed no clear bedding boundaries or grain size changes (Rosenthal et al., 2018; Table 2). At Site U1485, the massive layers are older and occur in two separate intervals (between ~210 and 230 ka and between ~235 and 280 ka; Table 2). Sandy silt corresponds to relatively thin, cm-thick beds (Figure 5D) that alternate with layers of *mud* and *silt* at meter and sub-meter scales. These alternations constitute the bulk of the sediments over the <~370 ka record (light grey bands in Figures 2, 3A and B). The *sandy silt* beds display a variety of sedimentologic structures (e.g. bottom

scouring, grading) and can include other components besides sand- and silt-size siliciclastics such as shell debris and coquina layers (Figure 5E), plant material (Figure 5F), and ash (Figure 5G).

LPSA sediment particle size distribution reflects the relative abundance of the sediment components that can be identified with smear slide analysis and thin section petrography (e.g. Aiello and Ravelo, 2012). At Sites U1484 and U1485, the silt- and sand-sized particles are mainly siliciclastic and include minerals, rock fragments and mineraloids. Minerals include angular to subangular feldspars (mainly K-feldspars and secondarily plagioclase feldspars), ferromagnesian minerals (mainly pyroxene and amphibole, whereas olivine occurs in trace amounts), and chlorite. Rock fragments are from volcanic rocks and, less commonly, intrusive plutonic and metamorphic rocks. Mineraloids are mainly represented by more or less pyritized glauconite that occurs as both irregular pelletal grains and transparent elongated fragments (Rosenthal et al., 2018). Sand- and silt-sized biogenic components consist primarily of whole or broken planktonic and benthic foraminifers and, together with brown plant material, they are common in the coarser-grained *sandy silt* but rare in the *silty sand*. Biogenic particles such as shell fragments, foraminifers, radiolarians, and nannofossils are mainly secondary components, although nannofossils can be abundant in the *mud* and *silt* especially in the younger part of the record.

Bivariate scattergrams can be used to interpret particle size parameters to characterize depositional environments (e.g. Mason and Folk, 1958; Lario et al. 2002; Brackenridge et al., 2018): mean grain size and sorting (SD) are hydraulically controlled, and these parameters tend to be positively correlated with the energy of the environment and the degree of sediment processing. When samples from Sites U1484 and U1485 are plotted on a bivariate scattergram (Figure 6), they display two opposite linear trends. For the fine-grained samples (mean size <~15μm; left of dashed line in Figure 6), standard deviation (SD) decreases with decreasing grain size, suggesting that sorting increases with decreasing energy conditions (Mason and Folk, 1958). This group includes mainly samples of *mud* and *silt* and most samples from the oldest, >~370 ka, part of Site U1485. For samples with mean sizes ranging between fine and medium silt, sorting increases with increasing mean size. This trend includes the samples of *sandy silt* and the coarsest

group of samples (*silty sand*; mean size  $>\sim$ 60 µm) with the latter displaying the highest sorting. The trend suggests preferential selection of coarser-grained particles with increasing energy conditions, which is a typical signature of channelized flows. Two groups of samples, outlined in Figure 6, are characterized by having the highest sorting: Group I includes samples from the last  $\sim$ 11 kyr (upper green bands in Figures 3A,B). Group II includes only samples from a massive sand layer recovered at Site U1485 between  $\sim$ 251 ka and  $\sim$ 255 ka (Figure 3B).

# 4.3 Particle Sizes vs. Sediment Properties

When correlated with sedimentologic characteristics such as sediment grain size distribution, the continuous physical property track data collected during IODP Expedition 363 provide a useful tool to extrapolate discrete sample measurements to the entire record at resolutions as fine as a few centimeters (representing hundreds of years). The shipboard track data used in this study are magnetic susceptibility (MS) and natural gamma radiation (NGR). Magnetic susceptibility records the magnetization induced in the material by an external magnetic field and provides information on the magnetic composition of the sediment that can commonly be related to mineralogical composition. Point-source magnetic susceptibility measurements were made on the archive halves of split-core sections at 2.5 cm spacing using dimensionless SI units, an IODP standard (Rosenthal et al., 2018). The NGR logger used during IODP Expedition 363 measures gamma radiation emitted from whole core sections every 10 cm. Gamma radiation derives primarily from the decay of mineral-hosted 238-uranium (238U), 232-thorium (232Th), and 40-potassium (40K) isotopes. In general, high counts identify fine-grained deposits containing K-rich clay minerals and their absorbed U and Th atoms (Serra, 1984). However, high NGR counts could also be due to high concentrations of authigenic U, which is enriched in sediments that are rich in organic material such as those that are deposited under anoxic conditions (Brumsack, 2006).

Bivariate plots of mean grain size vs. MS show that the variations in grain size populations explain approximately half (46%) of the variability of MS: the coarser the sediment the higher the magnetic mineral content ( $R^2 = 0.458$ ; p = 1.45e-39; Figure 7A). The sand percentage is positively correlated with

MS ( $R^2$  =0.487; p= 4.08e-63; Figure 7B). Conversely, the silt percentage ( $R^2$  = 0.406; p = 1.08e-49; Figure 7C) and clay percentage ( $R^2$  = 0.374; p = 8.07e-45; Figure 7D) are negatively correlated with MS suggesting that finer particles are poor magnetic carriers. There is weak negative correlation between mean grain size and NGR ( $R^2$  =0.237; p = 1.39e-23). NGR is correlated with the relative abundance of both clay- and silt-sized particles (Figures 8A–C). Percent clay explains approximately 26% of the variability ( $R^2$  = 0.257; p = 8.73e-26; Figure 8A). Note that the samples from >~300 ka cluster in a separate, high-%clay, high-NGR field. The correlation between %clay and NGR becomes slightly higher, when calculated separately for the younger part of the U1485 record ( $R^2$  = 0.285; p = 1.99e-23 for <~300 ka; Figure 8B), whereas there is no correlation for the older samples ( $R^2$  = 0.0537; P = 0.047 for >~300 ka; orange and yellow data points in Figure 8A). Percent silt is also positively correlated with NGR ( $R^2$  = 0.282; P = 1.5e-28; Figure 8C) and, as seen for %clay, the oldest (>~300 ka) samples have higher NGR and are grouped in a separate part of the bivariate plot. Conversely, %sand is negatively correlated with NGR ( $R^2$  = 0.315; P = 2.83e-32; Figure 8D).

#### 5 Discussion

The relationships between grain size, physical properties (MS, NGR) and lithologies at Sites U1484 and U1485 are interpreted in order to reconstruct the evolution of sedimentation on the continental margins of northern PNG since the middle Pleistocene. Since the sediments are mainly composed of siliciclastic particles, downhole variability in sediment characteristics can be interpreted in relation to changes in sediment sources, climate variability (e.g. intensity of precipitation and river discharge), and/or post-depositional processes, such as mass-gravity flows reworking the sediments once they reached the continental margins (Figure 10).

## 5.1 A Middle Pleistocene Epicontinental Sea (>~370 ka)

The fine-grained sediments that dominate between ~555 ka and ~370 ka at Site U1485 (Figures 3B and 9A) display the hallmarks of condensed 'pelagic mud' deposits found in continental margin

sequences worldwide (Loutit and Kennett, 1981; Galloway, 1989; Leckie et al., 1990). Relatively slow sedimentation rates (Figure 2), the linear negative relationship between sorting and mean grain size (Figure 6), low MS (Figure 7C, 7D and 9D), high NGR (Figures 8A, 8C and 9C) and the high abundance of nannofossils (Figure 6A) suggest sedimentation under low energy, oligotrophic conditions such as those characteristic of open ocean settings (Figure 11). Higher NGR values can sometimes be explained by sedimentation having occurred under anoxic conditions with higher preservation of organic matter and enrichment in authigenic U (Brumsack, 2006). However, there is no evidence that redox conditions were different than in the younger (<~370 ka) part of the record, since the average total organic carbon content (TOC) by weight for  $>\sim$ 370 ka (1.03%) is similar to the average TOC for  $<\sim$ 370 ka (0.92%; Rosenthal et al., 2018). Alternatively, higher NGR could reflect different concentrations, sources, and/or mineralogies of the detrital, clay- and silt-size fractions to which thorium (Th) and potassium (K) are linked (Brumsack, 2006). The deconvolution of the entire NGR spectra (counts as a function of gamma-ray energy level) can be used to estimate the sedimentary contribution of K, Th, and U from the characteristic gamma-ray energies of isotopes in the <sup>40</sup>K, <sup>232</sup>Th, and <sup>238</sup>U radioactive decay series (De Vleeschouwer et al., 2017). The deconvolved NGR spectra for Site U1485 (Supplementary Material Figure 2S) show that in the older (>~370 ka) portion of the sediment record the increase in NGR is mainly driven by the increase in Th relative to the other two elements: the concentration of Th is almost double that of the younger record (relative increase of ~90%), the relative increase of both K and U is only ~20%. High Th values can indicate the presence of heavy minerals (e.g. zircon, allanite, cheralite, monazite) resulting primarily from the weathering of siliceous igneous and metamorphic rocks. Due to its insolubility, Th is mostly transported in suspension and tends to concentrate in the silt fraction of shales (Brock, 1986; Serra, 1984). Th-rich heavy minerals may be derived from the upper watershed of the Sepik River in the westernmost New Guinea Highlands and/or the southern watershed of the Ramu River (e.g. Kubor Range), both characterized by extensive outcrops of Permian, Paleozoic and Triassic igneous and metamorphic basement rocks (Davies, 2012). Conversely, the coastal ranges, which are dominated by volcanic and sedimentary rocks, are mainly a source of K. The higher abundance of Th in the older part of

392

393

394

395

396

397

398

399

400

401

402

403

404

405

406

407

408

409

410

411

412

413

414

415

416

417

the record is, thus, compatible with a paleogeographic reconstruction that identifies the main source areas for the fine detrital fraction as the PNG interior. In contrast, the contribution from the coastal ranges was only minimal probably because before ~370 ka they were only partially uplifted and had smaller watersheds (Figure 11).

418

419

420

421

422

423

424

425

426

427

428

429

430

431

432

433

434

435

436

437

438

439

440

441

442

The dominance of marine sedimentation in western PNG since the late Miocene has been suggested by previous paleogeographic reconstructions for the region. While the western half of the modern Sepik Valley was either emergent or covered by shallow seas, deep marine sedimentation including pelagic marl facies was concentrated within three narrow troughs (Aitape, Lumi and Wewak) adjacent to the Bewani-Torricelli Fault System characterized by east-west oriented faults in the Bewani, Torricelli and Alexander Ranges in Figure 1, which was a rising and rapidly eroding mountain range (Hutchinson, 1975; Dow, 1977). Bathyal marine conditions have been suggested for the fine-grained sediments that constitute the bulk of the Wewak Beds, a formation that outcrops extensively in the Northern Ranges of PNG and beneath the Sepik-Ramu lowlands (Swadling et al., 1989; Chappell, 1993). Due to continued thrusting and uplift of the Northern Ranges, the epicontinental sea transitioned into a barred-basin inland sea later in the Pleistocene (Chappell, 1993). While the Northern Ranges were uplifting, the Sepik-Ramu region continued to subside, allowing the deposition of the marine sediments of the outer neritic Ouba Unit that has been recovered in exploratory wells in the Sepik Valley (Rogerson et al, 1987; Francis and Deibert, 1988). Both the sediments of the Ouba Unit (Swadling et al., 1989) and the pelagic marls facies of the Wewak Trough (Pawih, 1990) have been assigned to the upper part of nannofossil Zone NN19 of Martini (1971). These sediments are analogous in lithology and overlap in age with the sediments near the base of Site U1485, which are also assigned to the nannofossil Zone NN19 (Rosenthal et al., 2018). The pelagic marls of the Ouba Unit and the pelagic mud deposit of Site U1485 suggest that before ~370 ka only the finer fraction of the terrigenous input reached and accumulated on the continental margins because the rivers draining the New Guinea Highlands discharged directly into the epicontinental sea, further inland than today's location of the Sepik and Ramu River mouths (Figure 11).

### 5.2 From Ocean Inlet to River Valley

443

444

445

446

447

448

449

450

451

452

453

454

455

456

457

458

459

460

461

462

463

464

465

466

467

Starting at ~370 ka, pelagic mud was no longer the dominant sediment draping the northern continental margins of PNG, as indicated by the increase in mean grain size and higher MS (Figures 3B, 9A and 9D). This new sedimentary regime was characterized by background, hemipelagic deposition (mud and silt) periodically interrupted by cm- to tens-of-cm thick, coarser-grained beds (sandy silt; Figures 5H and 10). At Site U1485, a subset (92 beds) of the coarse-grained beds was selected for higher resolution grain size analysis (Supplementary Data). On the modified classification scheme of Folk (1954, 1974), most (77%) of the samples consist of sandy silt, and 33% of the samples fall in the coarser silty sand field (Figure 4B). None of the samples analyzed were identified as 'clean sand' (i.e. sand content >90%), which is typically found in turbidity-flow deposits. The identification of sedimentary structures, based on the visual interpretation of high-resolution digital photographs of 92 beds from which the high resolution samples were taken (Supplementary Material), shows that the majority of the beds (65%) have no obvious grading or evident changes in sediment texture from bottom to top (examples in Figure 5D and 10A), 15% show either evidence of reverse grading or the grain size increases towards the center of the bed (Figure 10B), whereas the proportion of the beds with normal grading is 20% (Figure 5H and 10C). Other common sedimentary structures identified include bottom scouring (Figure 10), the inclusion of brown plant matter (Figure 5F and 10C), coquina layers (Figures 5E, 10B and 10C) and ash layers (Figure 5G). Cross lamination was not observed, whereas faint parallel lamination was recorded mainly in homogenous or reverse graded beds (Figure 10B). Traditionally, gravity-flow deposits are differentiated based on the dominant sediment-support mechanism (turbulence vs. matrix), with the two end members being turbidity currents (turbidites) and debris flows (debrites; Middleton and Hampton, 1973). Hybrid conditions between end members include abrupt, progressive, or cyclical changes in flow behavior (e.g. turbulent versus laminar) during deposition and can occur genetically associated with turbidites (Filidani et al. 2018; Lowe and Guy, 2000; Hickson and Lowe, 2002; Talling et al., 2004; Haughton et al., 2009). Thus, we interpret that most of the matrix-rich sandy silt beds were derived from the deposition of hybridflows and not turbidity-flows, since these beds are generally massive or weakly graded and finer-grained than clean sand turbidites, and have larger proportions of silt and finer grains (Filidani et al. 2018).

The occurrence of coarser-grained siliciclastic sediments and sedimentation rates (up to ~0.1 cm/yr at Site U1484) that are similar to the modern sediment accumulation rates observed on the northwestern slope adjacent to the Sepik River delta (<0.2 cm/yr; Kuehl et al., 2004) suggest proximity/influence of river discharge to the continental margin, and the presence of mass-gravity flow deposits implies seafloor instability (Figure 11). In tectonically active and wet regions, the likelihood for massive failures triggering downslope transport increases during earthquakes or flood-stage flow in rivers (Mutti et al., 2013). In northwestern PNG, the rivers that were discharging coarse-grained sediments to the continental margins included not only the early tracks of the Sepik and Ramu Rivers but also other rivers that were draining the Northern Ranges, which were emergent at that time (Swalding et al., 1989). The uplift of the Northern Ranges also closed the troughs connecting the inland basin to the open ocean, leaving open only one connection between the Adalbert Range and the Northern Ranges, which still connects the Sepik and Ramu Rivers to the ocean today (Figure 11).

#### 5.3 The Last Three Glacial-Interglacial Cycles

The sedimentary record of the last ~300 kyr at both Sites U1484 and U1485 shows a general trend of increasing grain sizes during glacials followed by a return to fine-grained pelagic mud sedimentation after terminations, with the latter being the dominant lithofacies during the most extreme interglacial sea-level highstands (Figure 9G). This trend suggests that once the Sepik successor basin became a shallow, enclosed basin with only a restricted connection to the ocean, sea level change associated with glacial-interglacial-scale climate variability became an important mechanism controlling the position of the river mouth and the fate of fluvial sediments (Figure 11). River discharge to the continental margins was higher during lowstands associated with glacials, when the shoreline was closer to the modern shelf edge and the Sepik River eroded older floodplain and marine deposits and discharged them directly onto a narrow continental shelf. During interglacials, when sea level was high, only the finest clay- and silt-size

sediment fractions originating from the Sepik River were able to reach the continental margin, whereas the coarser-grained fraction was deposited closer to the river mouth, as the shoreline shifted further inland due to marine transgression.

493

494

495

496

497

498

499

500

501

502

503

504

505

506

507

508

509

510

511

512

513

514

515

516

517

Exceptions to this trend include the massive, coarser-grained events occurring asynchronously at the two sites, and the smaller, millennial-scale alternations between coarser- and finer-grained sediments (i.e. between sandy silt and mud and silt that account for the high-frequency MS variability since magnetization is mainly carried by the sand fraction (Figures 7B, 9D and 9E). High-frequency lithologic variability for the last 300 kyr was further explored with spectral analysis of the MS and NGR time-series from Site U1485 that was carried out with the Blackmann-Tuckey method using the AnalySeries 2.0 package (Paillard et al., 1996) with the following options: linear trend was removed and a Bartlett window was used with 80% confidence interval. Based on the statistical correlations with the grain size parameters (Figures 7 and 8), MS and NGR are interpreted as proxies for the contribution of coarsergrained terrigenous material from land and for the clay fraction, respectively. Spectral analysis of the MS record younger than 300 ka shows power concentrated at periodicities of 40 kyr and 23 kyr, corresponding to obliquity and precessional cycles (Supplementary Figure 3A). For NGR, the younger (<300 ka) portion of the record is characterized by a statistically significant correlation between NGR and both clay and silt percentages (Figures 8A, C); a high amplitude variability with a period of ~38 kyr, close to the period of obliquity, as well as a lower frequency peak at about 100 kyr are present (Supplementary Figure 3B).

Variations in XRF-derived Ti concentrations (both bulk and on a carbonate-free basis or Ti<sub>cfb</sub>) and in ln(Ti/Ca) in Core MD05-2920 were interpreted by Tachikawa et al., (2011) as proxies for coarse terrigenous input and river discharge from the Sepik and Ramu Rivers over the past 400 kyr. Bulk Ti concentration and ln(Ti/Ca) display high amplitude variations, corresponding to the obliquity (41 kyr) and precession (23 kyr) cycles, as well as an 11 kyr cycle, interpreted as a semi-precessional signal. Since Ti<sub>cfb</sub> displays only 23 kyr variability, Tachikawa et al. (2011) suggested that the 41 kyr cycle of bulk Ti

and ln(Ti/Ca) is mainly caused by biogenic carbonate contribution, which, in turn, is modulated by obliquity. Because of the strong coherency between these proxies and local summer insolation, Tachikawa et al. (2011) concluded that variations in terrigenous sediment content in Core MD05-2920 reflect mainly changes in precipitation at a precessional scale. Based on the antiphase relationship between the precipitation record and the Chinese speleothem  $\prod^{18}$ O records, which have been linked to the strength of the East Asian Summer monsoon (Wang et al., 2008; Figure 9F), less negative ⊓¹8O values imply lower summer monsoon rainfall in East Asia, with the ITCZ being displaced further south resulting in increased monsoon rainfall in the PNG region. Tachikawa et al. (2011) further suggested a close relationship between the Australian Monsoon and the East Asian Monsoon for at least the past 400 kyr. At Site U1485, MS shows high amplitude variability at the precession band, the presence of obliquity cycles in MS and NGR suggest that the input of coarse terrigenous sediments to the continental margins was controlled by both precession- and obliquity-driven processes. Our results are consistent with the REE to calcium (REE/Ca) ratios in the planktonic foraminifer Globigerinoides ruber from Core MD05-2925 (Liu et al., 2015), suggesting that during the last 282 kyr, the migration of the ITCZ was influenced by a combination of both precession and obliquity and not just precession. Based on the results of a coupled ocean-atmosphere model, Liu et al. (2015) hypothesized that obliquity forcing could be the result of cross-hemispherical thermal pressure contrast: at high obliquity, the ITCZ is 'pushed' further to the south over northern Australia, where precipitation increases while conditions in PNG are drier. Conversely, at low obliquity, the ITCZ is 'pulled' to the north and the PNG experiences enormous rainfall, especially during precessional highs in the southern hemisphere (Liu et al., 2105). Another difference is that, unlike the terrigenous proxies such as Ti in Core MD05-2920 (Tachikawa et al., 2011), the NGR record from Site U1485 (correlated with clay abundance, Figure 8B) exhibits 100

518

519

520

521

522

523

524

525

526

527

528

529

530

531

532

533

534

535

536

537

538

539

540

541

542

Another difference is that, unlike the terrigenous proxies such as Ti in Core MD05-2920 (Tachikawa et al., 2011), the NGR record from Site U1485 (correlated with clay abundance, Figure 8B) exhibits 100 kyr cyclicity. For the last ~300 kyr, each of the last four glacial terminations (TIV, TIII, TII and TI) and one "extra-termination" TIIIa (grey bars in Figure 9) are associated with stratigraphic intervals entirely dominated by *mud* and *silt* (green vertical bars in Figure 9), which coincide with extreme sea level

highstands during interglacials (Figure 9G). As recognized by previous authors (e.g. Loutit et al., 1988; Loutit and Kennett, 1981; Leckie et al., 1990; Galloway, 1989), drapes of hemipelagic and pelagic mud associated with maximum water depths during sea level transgression and/or highstands accumulate over lowstand deposits and are connected with the transgressive phase of a parasequence. When compared with the Chinese speleothem [180] record (Figure 9F; Wang et al., 2008), the five pelagic mud intervals occur both during times that follow glacial terminations when the ITCZ was displaced further north (more negative [180] values; after TI, TIIIa and TIII) and south (less negative [180] values; after TII and TIV). Hence, the pelagic mud intervals occur after each glacial termination whether the conditions over PNG were dry or wet, further supporting the interpretation that it was sea level transgression and not decreased precipitation that determined the siliciclastic sediment starvation to the continental margin and the deposition of the pelagic mud.

Sea level lowstands could have favored the flux of chemically weathered sediments from tropical shelf-slope riverine systems such as the Sepik-Ramu River system with potential implications for the global carbon cycle during the Pleistocene. A study by Wan et al. (2017), based on a 1.1 Myr record from two deep sea sites in the South China Sea (ODP Sites 1143 and 1144), shows that variations of proxy records for the intensity of silicate weathering (e.g. K/Al and K/Mg, kaolinite/illite and clay/feldspar) are correlated to glacial-interglacial-scale climate variability. Higher fluxes of chemically weathered sediments are associated with sea level lowstands and were interpreted by Wan et al. (2017) as the result of subaerial exposure and availability of larger volumes of unconsolidated shelf sediments during glacials for weathering. Wan et al. (2017) further hypothesized that because of the increased fluxes of chemically weathered sediments during sea level lowstands, tropical shelf-slope systems may have played a significant role in enhancing the drawdown of atmospheric  $pCO_2$  causing intensification of glacial cycles during the Pleistocene. Future studies on the relationships between sea level change and fluxes of chemically weathered siliciclastics in the sediment record from the continental margins of PNG will be crucial to test this hypothesis. Although the drainage area of the Sepik River (~80 x  $10^3$  km²; Milliman,

1995) is one order of magnitude smaller than the area of the Mekong River (the main source of riverine sediment to the South China Sea;  $\sim 80 \times 10^4 \text{ km}^2$ ; Liu et al., 2009), the volume of sediment delivered by the rivers draining the east coast of PNG is approximately twice that of the sediment yield from all the rivers flowing into the South China Sea ( $\sim 0.2 \times 10^9 \text{ Tons vs.} \sim 0.38 \times 10^9 \text{ Tons}$ ; Milliman and Meade, 1983).

Other controls on sediment fluxes to the continental margins associated with factors other than sea level and/or changes in precipitation cannot be excluded. For instance, the waxing and waning of montane glaciers in the PNG cordillera and related cycles of glacial erosion could have led to the formation of moraine deposits and cyclical fluxes of terrigenous sediments to the oceans (estimates of the extent of glaciers in PNG for the Last Glacial Maximum range between 3550 and 4000m above sea level; Prentice et al., 2005).

Proxy records for the last ~600 kyr across the equatorial Pacific Ocean show that Pleistocene productivity peaked at major glacial terminations and "extra terminations" (Winckler et al., 2016; Diz et al., 2018). During the deglacial productivity maxima, the contribution of Fe by upwelling was higher than eolian-driven Fe, thus excluding the dust fertilization hypothesis for the equatorial Pacific Ocean (Winckler et al., 2016). Rivers draining PNG, including the Sepik River, have been identified as a possible source of dissolved Fe carried across the ocean via the EUC and then upwelled in the equatorial Pacific (Milliman et al., 2009; Winckler et al., 2016). Overall, the sediment records of IODP Sites U1484 and U1485 show higher river discharge during glacials (e.g. higher MS and coarser grain sizes), supporting the hypothesis that the Sepik River is a potential source of Fe during these times. However, glacial terminations, the periods of highest productivity in the equatorial Pacific Ocean, do not systematically coincide with peak values of either MS or grain size that would suggest increased sediment discharge from PNG (Figures 9A, 9D and 9E).

# 5.4 Origin of Massive Sand Layers

Precession- and obliquity-scale changes in the intensity of the hydrological cycle and glacialinterglacial scale changes in sea level were not the only factors influencing the deposition of coarse terrigenous material on the continental margin of PNG. In active tectonic margins, seismic activity can also be a key factor in both increasing terrigenous inputs to the ocean due to seismic shaking and terrestrial landslides, as well as triggering submarine landslides or slumps and promoting resedimentation from mass-gravity flows. When plotted on Folk's (1954) modified ternary diagram, the majority (~60%) of the samples collected from 14 massive, homogenous, coarse-grained layers fall in the silty sand field (Figure 4C). The samples from these layers are also the most sorted and occur clustered in a separate. high-mean grain size, low-SD corner of the bivariate plot of Figure 6 (Group II). Another unique characteristic of the massive sand deposits is that while the hybrid flow deposits occur in relatively thin beds, these layers can be up to several meters thick and they generally form lithologically homogenous intervals (Figure 5C). In some cases, the massive layers include mottles of clay that can be interpreted as rip-up clasts suggesting the amalgamation of multiple events that occurred over intervals of tens of thousands of years (Table 2; Figure 3). The lithologic and sedimentologic characteristics of the massive silty sand layers are compatible with Mulder and Alexander's (2001) description for frictional subaqueous hyperconcentrated grain flows typical of channelized flow conditions. In these flows the space between grains is filled mainly by water and not by a sediment matrix. The fluid has no cohesion but grain-to-grain interactions support and transport the sediment load. While the depositional product of hyperconcentrated flows could show some basal inverse grading, neither normal grading nor bedforms are usually preserved. The timing of the massive grain-flow deposits is different at the two sites. At Site U1485, they occur earlier and cluster in two separate intervals between ~280 and ~235 ka and between ~230 and ~210 ka (Figure 3B; Table 2). At Site U1484, the grain-flow deposits occur later and have a shorter duration

592

593

594

595

596

597

598

599

600

601

602

603

604

605

606

607

608

609

610

611

612

613

614

615

616

(between ~140 and ~192 ka; Figure 3A; Table 2). These deposits can be interpreted to result from repeated failures of shallow continental margin areas. The failures occurred repeatedly over tens of thousands of years since not only is there no evidence of unconformities or condensed sedimentation, but these deposits correspond to the fastest sedimentation rates recorded at the sites (Figure 2). Under this scenario, the seafloor failures produced channelized, downslope transport (e.g. along submarine canyons) of shelf material. The triggers for the failures could have been large earthquakes since the trace of the BSSL intersects the coastline in the immediate vicinity of Sites U1484 and U1485 (Figure 1). The region has been affected by the devastating effects of two major tsunami events in recent years (1998 and 2002) that were associated with strong earthquakes (Ms7.0 and 7.8, respectively) with epicenters located off the northern coast of the East Sepik Province (Kawata et al., 1999; Borrero, 2002). The tsunamis were probably triggered by underwater landslides or slumps potentially identified by subsequent offshore surveys (Tappin et al., 1999; Sweet and Silver, 2003).

One of the shortcomings of interpreting the massive deposits as downslope mass failures, which would have occurred over tens of thousands of years, is that they should have occurred synchronously since Site U1485 is located just a few kilometers offshore and directly downslope from Site U1484. An alternative interpretation is that the submarine landslides that generated the grain flows occurred in more distal locations of the continental margins and that the hyperconcentrated flows migrated along marginparallel channels rather than downslope. The latter hypothesis is supported by swath bathymetry of the northwestern continental margin of PNG, which shows prominent, fault-controlled, northwest-trending, margin-parallel channels including one between ~1200 and 1400 m water depth just offshore Site U1485 (Figure 11). The channel can be traced for ~50 km to the northwest of Sites U1484 and U1485, where it crosses and offsets the Yalingi Canyon (Sweet and Silver, 2003). The interpretation of seismic reflection data by Sweet and Silver (2003) demonstrates that these margin-parallel channels (not unlike many other features of the continental margin) include slumping, normal faulting and uplifted blocks and are the result of an oblique subduction environment that includes both extensional and compressional features. The continental margin just northwest of the location of the two sites is essentially sediment starved and the continental slope, which dips 10-12°, has only a thin veneer of unconsolidated sediment (Sweet and Silver, 2003; Rosenthal et al., 2018). The thickest sediment imaged nearshore by Sweet and Silver (2003) is within a basin surrounding the head of Yalingi Canyon and could be one of the potential sources of the grain flows at Site U1485 (asterisk in Figure 1).

Whether the sources of the grain flows were local or distal and whether the channelized flows occurred along channels that were running perpendicular or parallel to the margin, the presence of these massive deposits suggests intensified tectonic activity along the northern continental margins of PNG over a period of ~140 kyr. The activity started at ~280 ka and ended at ~140 ka when the Northern Ranges were uplifting and the Sepik Basin was progressively shoaling (Figure 11).

#### 6 Conclusions

The sedimentologic analyses of Sites U1484 and U1485 presented in this study suggest that caution should be used when interpreting variations of the terrigenous components of a core record (e.g. %sand, MS, elemental ratios such as Ti/Ca or REE/Ca ratios) as straightforward indicators of the strength of the hydrological cycle, which, in the tropical regions, is mainly controlled by the position of the ITCZ. In successor basins formed after tectonic collisions such as the Sepik, sediment accumulation starts after the cessation of basin-controlling processes, and the basin acts as a trap for sediments until it is filled and then bypassed (Ingersoll, 2011). The exclusive deposition of pelagic mud on the continental margins prior to ~370 ka occurred because much of the sediment discharge from the rivers that were draining the New Guinea Highlands (including a "proto" Sepik River) was captured before reaching the ocean by an epicontinental sea that occupied the location of the modern Sepik Valley, not because climate was drier.

The PNG core record of Site U1485 confirms previous interpretations whereby precipitation in the tropical region of the Indonesian Archipelago was modulated by precession and obliquity. However, the PNG core record also shows that on a tropical island, glacial-interglacial scale cycles also have a significant influence on where riverine sediment is deposited. For the last ~300 kyr, after it became filled with sediments, the Sepik successor basin was directly affected by global variations in sea level: during sea level lowstands the Sepik River cut into previously deposited marine and nonmarine sediments and

discharged further offshore directly onto the shallow continental margins, producing seafloor instability and promoting mass-gravity flows. Conversely, during the most extreme highstand conditions following deglaciations, the mouth of the Sepik River was positioned further inland, away from the shelf. The shallow internal basin reverted back to marine conditions and river discharge was confined to the basin causing silt/sand starvation on the continental margins and a return to pelagic mud sedimentation under both high- and low-rainfall conditions, hence irrespective of the mean position of the ITCZ and of the strength of the hydrological cycle.

Finally, this study suggests that tectonics played multiple roles in the evolution of the region. On one side, the filling of the Sepik basins was accelerated by the uplift of the coastal ranges; not only because they provided further sources of terrigenous sediments to the internal basin, but also because they acted as barriers that further isolated the basins from the open ocean. Tectonic activity also had a major role in post-depositional resedimentation processes on the continental margin. The occurrence of massive grainflow deposits indicates a long period of heightened seismicity between ~280 ka and ~140 ka. The comparison of massive grain flow deposits at Sites U1484 and U1485 also suggests that in strike-slip systems in which fault-controlled submarine canyons and channels develop, both across and along the margins, mass-gravity flows can move both downslope and alongslope.

#### 7 References

- Aiello, I.W. and Ravelo, A.C., 2012. Evolution of marine sedimentation in the Bering Sea since the Pliocene. *Geosphere*, 8(6), pp.1231-1253.
- Abbott LD, Silver EA, Galewsky J., 1994. Structural evolution of a modern arc-continent collision in Papua New Guinea. *Tectonics* 13:1007–1034.
  - Amante, C. and B.W. Eakins, 2009. ETOPO1 1 Arc-Minute Global Relief Model: Procedures, Data Sources and Analysis. NOAA Technical Memorandum NESDIS NGDC-24. National Geophysical Data Center, NOAA. doi:10.7289/V5C8276M [2018].

- Baldwin, S.L., Fitzgerald, P.G. and Webb, L.E., 2012. Tectonics of the New Guinea region. *Annual*
- 691 Review of Earth and Planetary Sciences, 40, pp.495-520.
- Beaufort, L., Van der Kaars, S., Bassinot, F.C. and Moron, V., 2010. Past dynamics of the Australian
- monsoon: precession, phase and links to the global monsoon concept. Climate of the Past, 6, pp.695-706.
- 694 Beckman Coulter Inc., 2003. LS 13 230 Particle Size Analyzer Manual PN 7222061A. Particle
- 695 Characterization Group, Miami, Florida.
- Bird, M.I., Austin, W.E., Wurster, C.M., Fifield, L.K., Mojtahid, M. and Sargeant, C., 2010.
- Punctuated eustatic sea-level rise in the early mid-Holocene. *Geology*, 38(9), pp.803-806.
- Borrero, J.C., Bu, J., Saiang, C., Uslu, B., Freckman, J., Gomer, B., Okal, E.A. and Synolakis, C.E.,
- 699 2003. Field survey and preliminary modeling of the Wewak, Papua New Guinea earthquake and tsunami
- of 9 September 2002. Seismological Research Letters, 74(4), pp.393-405.
- Brackenridge, R.E., Stow, D.A., Hernández-Molina, F.J., Jones, C., Mena, A., Alejo, I., Ducassou,
- 702 E., Llave, E., Ercilla, G., Nombela, M.A. and Perez-Arlucea, M., 2018. Textural characteristics and facies
- of sand-rich contourite depositional systems. *Sedimentology*, 67(7), pp.2223-2252.
- Brock, J. (1986). Applied open-hole log analysis. Petro-Media, Tyler, TX.
- 705 Brumsack, H.J., 2006. The trace metal content of recent organic carbon-rich sediments: implications
- for Cretaceous black shale formation. Palaeogeography, Palaeoclimatology, Palaeoecology, 232(2-4),
- 707 pp.344-361.
- Cane, M.A. and Molnar, P., 2001. Closing of the Indonesian seaway as a precursor to east African
- aridification around 3–4 million years ago. *Nature*, 411(6834), p.157.
- 710 Chappell, J., 1993. Contrasting Holocene sedimentary geologies of lower Daly River, northern
- Australia, and lower Sepik-Ramu, Papua New Guinea. Sedimentary Geology, 83(3-4), pp.339-358.

- Cheng, H., Sinha, A., Wang, X.F. & Cruz, F.W., 2012. The global paleomonsoon as seen through
- speleothem records from Asia and South America. *Clim. Dyn.* 39, pp.1045-1062.
- Cheng, H., Edwards, R.L., Sinha, A., Spötl, C., Yi, L., Chen, S., Kelly, M., Kathayat, G., Wang, X.,
- Li, X. and Kong, X., 2016. The Asian monsoon over the past 640,000 years and ice age
- 716 terminations. *Nature*, *534*(7609), p.640.
- 717 Clift, P.D. (2006) Controls on the Erosion of Cenozoic Asia and the Flux of Clastic Sediment to the
- Ocean. Earth and Planetary Science Letters, 241, pp.571-580.
- Clift, P.D., Giosan, L., Blusztajn, J., Campbell, I.H., Allen, C.M., Pringle, M., Tabrez, A., Danish,
- M., Rabbani, M.M., Carter, A. & Lückge, A. (2008) Holocene Erosion of the Lesser Himalaya Triggered
- by Intensified Summer Monsoon. *Geology*, 36, pp.79-82.
- Cloos, M., B. Sapiie, A. Quarles van Ufford, R. J. Weiland, P. Q. Warren, and T. P. McMahon,
- 723 2005. Collisional Delamination in New Guinea: The Geotectonics of Subducting Slab Breakoff, Spec.
- 724 Pap., vol. 400, 51 pp., Geol. Soc. Am., Boulder, Colo.
- 725 Cooper P, Taylor B. 1987. Seismotectonics of New Guinea: a model for arc reversal following arc-
- 726 continent collision. *Tectonics* 6, pp.53 -67
- 727 Cresswell, G.R., 2000. Coastal currents of northern Papua New Guinea, and the Sepik River
- outflow. *Marine and Freshwater Research*, 51(6), pp.553-564.
- 729 Crowhurst, P.V., Hill, K.C., Foster, D.A. and Bennett, A.P., 1996. Thermochronological and
- 730 geochemical constraints on the tectonic evolution of northern Papua New Guinea. *Geological Society*,
- 731 London, Special Publications, 106(1), pp.525-537.
- Cruz Jr, F.W., Burns, S.J., Karmann, I., Sharp, W.D., Vuille, M., Cardoso, A.O., Ferrari, J.A., Dias,
- P.L.S. and Viana Jr, O., 2005. Insolation-driven changes in atmospheric circulation over the past 116,000
- years in subtropical Brazil. *Nature*, 434(7029), p.63.

- 735 Davies, H.L., 2012. The geology of New Guinea—the cordilleran margin of the Australian
- continent. Episodes-Newsmagazine of the International Union of Geological Sciences, 35(1), p.87.
- De Vleeschouwer, D., Dunlea, A. G., Auer, G., Anderson, C. H., Brumsack, H., de Loach, A., ... &
- Kominz, M. A. (2017). Quantifying K, U, and Th contents of marine sediments using shipboard natural
- gamma radiation spectra measured on DV JOIDES Resolution. Geochemistry, Geophysics,
- 740 Geosystems, 18(3), 1053-1064.
- Diz, P., Hernández-Almeida, I., Bernárdez, P., Pérez-Arlucea, M. and Hall, I.R., 2018. Ocean and
- atmosphere teleconnections modulate east tropical Pacific productivity at late to middle Pleistocene
- 743 terminations. Earth and Planetary Science Letters, 493, pp.82-91.
- Dow, D.B., 1977. A geological synthesis of Papua New Guinea (Vol. 201). Australian Government
- Publ. Service, 41 p.
- Fildani, A., Clark, J., Covault, J.A., Power, B., Romans, B.W. and Aiello, I.W., 2018. Muddy sand
- and sandy mud on the distal Mississippi fan: Implications for lobe depositional
- 748 processes. *Geosphere*, 14(3), pp.1051-1066.
- Fine, R.A., Lukas, R., Bingham, F.M., Warner, M.J. and Gammon, R.H., 1994. The western
- 750 equatorial Pacific: A water mass crossroads. Journal of Geophysical Research: Oceans, 99(C12),
- 751 pp.25063-25080.
- Folk, R.L., 1954, The distinction between grain size and mineral composition in sedimentary-rock
- 753 nomenclature. The Journal of Geology, 62, p.344-359, https://doi.org/10.1086/626171.
- Folk, R.L., 1974, Petrology of Sedimentary Rocks: Austin, Texas, Hemphill Publishing Company,
- 755 182 p.
- Francis, G., Deibert, D.H., Hartung-Kagi, B., Warrillow, C., Perembo, R. and Hekel, H.K.,
- 757 1988. Petroleum Potential of the North New Guinea Basin and Associated Infrabasins. Geological Survey
- of Papua New Guinea, 229 p.

- Gaillardet, J., Dupré, B., Louvat, P. and Allegre, C.J., 1999. Global silicate weathering and CO2
- consumption rates deduced from the chemistry of large rivers. *Chemical Geology*, 159(1-4), pp.3-30.
- Galloway, W.E., 1989. Genetic stratigraphic sequences in basin analysis I: architecture and genesis
- of flooding-surface bounded depositional units. AAPG bulletin, 73(2), pp.125-142.
- Hamilton W. 1979. Tectonics of the Indonesian Region. Washington, DC: US Gov. Print. Off. 345
- 764 pp.
- Hall, R., 2002. Cenozoic geological and plate tectonic evolution of SE Asia and the SW Pacific:
- computer-based reconstructions, model and animations. Journal of Asian Earth Sciences, 20(4), pp.353-
- 767 431.
- Haughton, P.D.W., Davies, C.E., and McCaffrey, W.D., 2009, Hybrid sediment gravity flow
- deposits: Classification, origin and significance. Marine and Petroleum Geology, 26, p.1900-1918,
- 770 https://doi.org/10.1016/j.marpetgeo.2009.02.012.
- Hickson, T.A., and Lowe, D.R., 2002, Facies architecture of a submarine fan channel-levee com-
- 772 plex: The Juniper Ridge Conglomerate, Coalinga, California. Sedimentology, 49, p.335-362,
- 773 https://doi.org/10.1046/j.1365-3091.2002.00447.x.
- Hill K.C., Hall R., 2003. Mesozoic-Cenozoic evolution of Australia's New Guinea margin in a west
- 775 Pacific context. *Geol. Soc. Am. Spec. Pap.*, 372, pp.265-290.
- Hill KC, Raza A. 1999. Arc-continent collision in Papua Guinea: constraints from fission track
- thermochronology. *Tectonics*, 18, pp.950–966.
- Holm, R.J. and Richards, S.W., 2013. A re-evaluation of arc-continent collision and along-arc
- variation in the Bismarck Sea region, Papua New Guinea. Australian Journal of Earth Sciences, 60(5),
- 780 pp.605-619.

- Hutchinson, D. S., 1975. Basement geology of the North Sepik region, *Bur. Miner. Resour. Aust.*
- 782 Rec., 162.
- 783 International Seismological Centre, 2016. *Online* Bulletin, http://www.iisc.ac.uk, Internal. Seismol.
- 784 Cent., Thatcham, United Kingdom.
- Jacques, A.L., 1977. The continent-arc collision in northern Papua New Guinea. *BRMJ. Aust. Geol.*
- 786 *Geophys.*, 2, pp.289-303.
- Kawata, Y., Benson, B.C., Borrero, J.C., Borrero, J.L., Davies, H.L., de Lange, W.P., Imamura, F.,
- Letz, H., Nott, J. and Synolakis, C.E., 1999. Tsunami in Papua New Guinea was as intense as first
- thought. Eos, Transactions American Geophysical Union, 80(9), pp.101-105.
- Kineke, G.C., Woolfe, K.J., Kuehl, S.A., Milliman, J.D., Dellapenna, T.M. and Purdon, R.G., 2000.
- 791 Sediment export from the Sepik River, Papua New Guinea: evidence for a divergent sediment
- 792 plume. Continental Shelf Research, 20(16), pp.2239-2266.
- Konert, M., and Vandenberghe, J., 1997, Comparison of laser grain size analysis with pipette and
- sieve analysis: A solution for the underestimation of the clay fraction. Sedimentology, 44, pp.523-535,
- 795 https://doi.org/10.1046/j.1365-3091.1997.d01-38.x.
- Kuehl, S.A., Brunskill, G.J., Burns, K., Fugate, D., Kniskern, T. and Meneghini, L., 2004. Nature of
- sediment dispersal off the Sepik River, Papua New Guinea: preliminary sediment budget and implications
- for margin processes. *Continental Shelf Research*, 24(19), pp.2417-2429.
- Kuroda, Y., 2000. Variability of currents off the northern coast of New Guinea. *Journal of*
- 800 *Oceanography*, 56(1), pp.103-116.
- Lario, J., Spencer, C., Plater, A.J., Zazo, C., Goy, J.L. and Dabrio, C.J., 2002. Particle size
- 802 characterisation of Holocene back-barrier sequences from North Atlantic coasts (SW Spain and SE
- 803 England). *Geomorphology*, 42(1-2), pp.25-42.

- Leckie, D.A., Singh, C., Goodarzi, F. and Wall, J.H., 1990. Organic-rich, radioactive marine shale; a
- case study of a shallow-water condensed section, Cretaceous Shaftesbury Formation, Alberta,
- 806 Canada. Journal of Sedimentary Research, 60(1), pp.101-117.
- Liu, S., Lu, P., Liu, D., Jin, P. and Wang, W., 2009. Pinpointing the sources and measuring the
- lengths of the principal rivers of the world. *International Journal of Digital Earth*, 2(1), pp.80-87.
- 809 Liu, Y., Lo, L., Shi, Z., Wei, K.Y., Chou, C.J., Chen, Y.C., Chuang, C.K., Wu, C.C., Mii, H.S.,
- Peng, Z. and Amakawa, H., 2015. Obliquity pacing of the western Pacific Intertropical Convergence Zone
- over the past 282,000 years. *Nature Communications*, 6, p.10018.
- 812 Liu, J.P., DeMaster, D.J., Nguyen, T.T., Saito, Y., Nguyen, V.L., Ta, T.K.O. and Li, X., 2017.
- 813 Stratigraphic formation of the Mekong River Delta and its recent shoreline
- 814 changes. *Oceanography*, 30(3), pp.72-83.
- Loutit, T.S., Hardenbol, J., Vail, P.R. and Baum, G.R., 1988. Condensed sections: the key to age
- determination and correlation of continental margin sequences. Spec. Publ. Soc. Econ. Paleont. Miner.,
- 817 *42*, pp.183-213.
- Loutit, T.S. and Kennett, J.P., 1981. New Zealand and Australian Cenozoic sedimentary cycles and
- global sea-level changes. AAPG Bulletin, 65(9), pp.1586-1601.
- 820 Lowe, D.R., and Guy, M., 2000, Slurry-flow deposits in the Britannia Formation (Lower
- 821 Cretaceous), North Sea: A new perspective on the turbidity current and debris flow problem: Sedimentol-
- 822 ogy, v. 47, p. 31–70, https://doi.org/10.1046/j.1365-3091.2000.00276.x.
- Martin, J.H., 1992. Iron as a limiting factor in oceanic productivity. In Falkowski P.G., Woodhead
- 824 A.D., Vivirito K. (eds) *Primary productivity and biogeochemical cycles in the sea* (pp. 123-137).
- 825 Environmental Science Research, 43. Springer, Boston, MA.
- Martinez F, Taylor B. 1996. Backarc spreading, rifting, and microplate rotation, between transform
- faults in the Manus basin. Mar. Geophys. Res., 18, pp-203-24.

- Martini, E. 1971. Standard Tertiary and Quaternary calcareous nannoplankton zonation. *Proceedings*
- of the Second Planktonic Conference, Roma 1970, pp.739-785.
- Mason, C.C. and Folk, R.L., 1958. Differentiation of beach, dune, and aeolian flat environments by
- size analysis, Mustang Island, Texas. *Journal of Sedimentary Research*, 28(2), pp.211-226.
- McCave, I.N., Hall, I.R., and Bianchi, G.G., 2006, Laser vs. settling velocity differences in silt grain-
- 833 size measurements: Estimation of palaeocurrent vigor. Sedimentology, 53, pp.9198928,
- 834 https://doi.org/10.1111/j.1365-3091.2006.00783.x.
- Milliman, J.D. and Meade, R.H., 1983. World-wide delivery of river sediment to the oceans. *The*
- 836 *Journal of Geology*, 91(1), pp.1-21.
- Milliman, J.D. and Syvitski, J.P., 1992. Geomorphic/tectonic control of sediment discharge to the
- ocean: the importance of small mountainous rivers. *The Journal of Geology*, 100(5), pp.525-544.
- Milliman, J.D., 1995. Sediment discharge to the ocean from small mountainous rivers: the New
- Guinea example. *Geo-Marine Letters*, 15(3-4), pp.127-133.
- Milliman, J.D., Farnsworth, K.L. and Albertin, C.S., 1999. Flux and fate of fluvial sediments leaving
- large islands in the East Indies. *Journal of Sea Research*, 41(1-2), pp.97-107.
- Molnar, P. and Cronin, T.W., 2015. Growth of the Maritime Continent and its possible contribution
- to recurring Ice Ages. *Paleoceanography*, 30(3), pp.196-225.
- Mountain, G.S., Burger, R.L., Delius, H., Fulthorpe, C.S., Austin, J.A., Goldberg, D.S., Steckler,
- 846 M.S., McHugh, C.M., Miller, K.G., Monteverde, D.H. and Orange, D.L., 2007. The long-term
- 847 stratigraphic record on continental margins. Continental margin sedimentation: From sediment transport
- to sequence stratigraphy: International Association of Sedimentologists Special Publication, 37, pp.381-
- 849 458.

- Mulder, T. and Alexander, J., 2001. The physical character of subaqueous sedimentary density flows
- and their deposits. *Sedimentology*, 48(2), pp.269-299.
- Nittrouer, C.A., Mullarney, J.C., Allison, M.A. and Ogston, A.S., 2017. Sedimentary processes building a
- tropical delta yesterday, today, and tomorrow: The Mekong system. *Oceanography*, 30(3), pp.10-21.
- Paillard, D., Labeyrie, L., Yiou, P., 1996. Macintosh program performs time-series analysis. *EOS*
- 855 Trans. AGU, 77.
- Pawih, B., 1990. Stratigraphy and tectonics of the Wewak Trough. Papua New Guinea (PNG). In
- 857 Carman, G.J. and Z., (Eds), Petroleum Exploration in Papua New Guinea. Proceedings of the First PNG
- Petroleum Convention, Port Moresby, 12-14th Feb, pp.491-498.
- Pegler G, Das S, Woodhouse JH. 1995. A seismological study of the eastern New Guinea and
- western Solomon Sea regions and its tectonic implications. *Geophys. J. Int.*, 122, pp-961-81.
- Prentice, M.L., Hope, G.S., Maryunani, K. and Peterson, J.A., 2005. An evaluation of snowline data
- across New Guinea during the last major glaciation, and area-based glacier snowlines in the Mt. Jaya
- region of Papua, Indonesia, during the Last Glacial Maximum. *Quaternary International*, 138, pp.93-117.
- Ripper, I.D., 1980. Seismicity, earthquake focal mechanisms and tectonics of the Indo-
- Australian/Solomon Sea plate boundary. **Dept of Min. and Energy Rep. 8015,** Geol. Surv. Papua New
- 866 Guinea, Port Moresby.
- 867 Rogerson, R.J., Hilyard, D.B., Finlayson, E.J., Holland, D.J., Nion, S.T.S., Sumaiang, R.M.,
- 868 Duguman, J. and Loxton, C.D.C., 1987. The geology and mineral resources of the Sepik Headwaters
- 869 region, Papua New Guinea, Dept of Min. and Energy Rep., Geol. Surv. Papua New Guinea, Port
- 870 Moresby, 130 p.
- Rosenthal, Y., Holbourn, A.E., Kulhanek, D.K., and the Expedition 363 Scientists, 2018. Western
- 872 Pacific Warm Pool. Proceedings of the International Ocean Discovery Program, 363: College Station, TX
- 873 (International Ocean Discovery Program). https://doi.org/10.14379/iodp.proc.363.2018.

- 874 Serra, O., 1984, 7. Natural Gamma-Ray Spectrometry, in Developments in Petroleum Science, edited
- by O. Serra, pp. 113–134, Elsevier, Amsterdam, The Netherlands.
- Singer, J.K., Anderson, J.B., Ledbetter, M.T., McCave, I.N., Jones, K.P.N., and Wright, R., 1988,
- An assessment of analytical techniques for the size analysis of fine-grained sediments. *Journal of*
- 878 *Sedimentary Research*, 58, pp.534-543, https://doi.org/10.1306/212F8DE6-2B24-11D7 -
- 879 8648000102C1865D.
- Spratt, R.M. and Lisiecki, L.E., 2016. A Late Pleistocene sea level stack. *Climate of the Past*, 12(4),
- 881 pp.1079-1092.
- Stanley DJ, Warne AG., 1994. Worldwide initiation of Holocene marine deltas by deceleration of
- sea-level rise. *Science*, 265(5169), pp.228-31.
- Swadling, P., Chappell, J., Francis, G., Araho, N. and Ivuyo, B., 1989. A Late Quaternary inland sea
- and early pottery in Papua New Guinea. Archaeology in Oceania, 24(3), pp.106-109.
- 886 Sweet, S. and Silver, E.A., 2003. Tectonics and slumping in the source region of the 1998 Papua
- New Guinea tsunami from seismic reflection images. In Landslide Tsunamis: Recent Findings and
- 888 Research Directions (pp. 1945-1968). Birkhäuser, Basel.
- Tachikawa, K., Cartapanis, O., Vidal, L., Beaufort, L., Barlyaeva, T. and Bard, E., 2011. The
- precession phase of hydrological variability in the Western Pacific Warm Pool during the past 400
- 891 ka. Quaternary Science Reviews, 30(25-26), pp.3716-3727.
- Talling, P.J., Masson, D.G., Sumner, E.J., and Malgesini, G., 2012, Subaqueous sediment density
- flows: Depositional processes and deposit types. Sedimentology, 59, pp.1937-2003, https://
- 894 doi.org/10.1111/j.1365-3091.2012.01353.x.
- Tappin, D.R., Matsumoto, T., Watts, P., Satake, K., McMurtry, G.M., Matsuyama, M., Lafoy, Y.,
- 896 Tsuji, Y., Kanamatsu, T., Lus, W. and Iwabuchi, Y., 1999. Sediment slump likely caused 1998 Papua
- New Guinea tsunami. Eos, Transactions American Geophysical Union, 80(30), pp.329-340.

- Taylor B. 1979. Bismarck Sea: evolution of a back-arc basin. *Geology*, 7, pp.171-74.
- Tregoning P, Jackson RJ, McQueen H, Lambeck K, Stevens C, et al. 1999. Motion of the South
- 900 Bismarck Plate, Papua New Guinea. *Geophys. Res. Lett.*, 26, pp.3517-20.
- Viers, J., Dupré, B. and Gaillardet, J., 2009. Chemical composition of suspended sediments in World
- Rivers: New insights from a new database. Science of the total environment, 407(2), pp.853-868.
- Wallace LM, Stevens C, Silver E, McCaffrey R, Loratung W, et al. 2004. GPS and seismological
- on straints on active tectonics and arc-continent collision in Papua New Guinea: implications for
- mechanics of microplate rotations in a plate boundary zone. J. Geophys. Res., 109:B05404
- Wan, S., Clift, P.D., Zhao, D., Hovius, N., Munhoven, G., France-Lanord, C., Wang, Y., Xiong, Z.,
- 907 Huang, J., Yu, Z. and Zhang, J., 2017. Enhanced silicate weathering of tropical shelf sediments exposed
- during glacial lowstands: A sink for atmospheric CO2. Geochimica et Cosmochimica Acta, 200, pp.123-
- 909 144.
- Wang, Y., Cheng, H., Edwards, R.L., Kong, X., Shao, X., Chen, S., Wu, J., Jiang, X., Wang, X. and
- An, Z., 2008. Millennial-and orbital-scale changes in the East Asian Monsoon over the past 224,000
- 912 years. *Nature*, 451(7182), p.1090.
- Weiler, P.D. and Coe, R.S., 2000. Rotations in the actively colliding Finisterre Arc Terrane:
- paleomagnetic constraints on Plio-Pleistocene evolution of the South Bismarck microplate, northeastern
- 915 Papua New Guinea. *Tectonophysics*, *316*(3-4), pp.297-325.
- 916 Winckler, G., Anderson, R.F., Jaccard, S.L. and Marcantonio, F., 2016. Ocean dynamics, not dust,
- have controlled equatorial Pacific productivity over the past 500,000 years. *Proceedings of the National*
- 918 Academy of Sciences, 113(22), pp.6119-6124.
- Woodhead JD, Hergt J, Sandiford M, Johnson W. 2010. The big crunch: physical and chemical
- expressions of arc/continent collision in the Western Bismarck arc. J. Volcanol. Geotherm. Res., 190,
- 921 pp.11-24.

Zhang, Z., Tyrrell, S., Li, C.A., Daly, J.S., Sun, X., Blowick, A. and Lin, X., 2016. Provenance of detrital K-feldspar in Jianghan Basin sheds new light on the Pliocene–Pleistocene evolution of the Yangtze River. *Bulletin*, *128*(9-10), pp.1339-1351.

## 8 Supplementary data

Figure S1: Benthic foraminifer oxygen isotope records from IODP Sites U1484 (purple) measured on *Cibicidoides pachyderma* and U1485(red) measured on *Uvigerina peregrina* relative to the LR04 benthic stack (black) (Lisiecki and Raymo, 2005). The age models for Sites U1484 and U1485 are based on correlation of the oxygen isotope records from each site to the LR04 benthic stack, with 8 and 13 tie points defined, respectively. Tie points are provided in the Supplemental Material (Table 1a, 1b). Four radiocarbon dates provide additional age constraints over the most recent 30 kry at Site U1485.

- Figure S2: Deconvolved NGR spectra for IODP Hole U1485A.
- Figure S3: Results of Blackman-Tukey spectral analysis including 80% confidence interval for IODP

  Hole U1485A for the last 300 kyr: A) magnetic susceptibility; B) natural gamma radiation.
- Table S1: Age models tie points used for A) IODP Site U1484 and B) IODP Site U1485.

## 9 Figures

Figure 1: Map of northeastern PNG with location of IODP Sites U1484 and U1485 and piston Core MD05-2920 (Tachikawa et al., 2011). The map includes: terrain and bathymetric models (ETOPO1; Amante and Eakins, 2009), earthquake epicenters (M>2.5; red crosses) between 2000 and 2018 (International Seismological Centre, 2016), main onshore and offshore tectonic structures and plate boundaries (from Dow, 1977; Holm and Richards, 2013; Baldwin 2012). The asterisk indicates the approximate position of the Yalingi Canyon (Sweet and Silver, 2003). The inset map also includes main surface (solid line) and intermediate water (dashed lines) oceanic current systems (NGCUC = New

Guinea Coastal Counter Current; NGCC = New Guinea Coastal Current; EUC = Equatorial Under Current; from Cresswell, 2000).

Figure 2: Age vs. depth plot (Core Composite Depth Below Sea Floor or CCSF; Rosenthal et al., 2018) for IODP Sites U1484 (red) and U1485 (black). The colored bars represent stratigraphic intervals dominated by sediment textures that can be correlated across the two sites (only for <317 ka). The green bands correspond to stratigraphic intervals dominated by fine-grained sedimentation (Table 2; see text for further details). The asterisks correspond to intervals characterized by massive, mainly *silty sand*, deposits that have been interpreted as grain-flows and that occur at different times in the two sites.

Figure 3: Lithologic sketches for IODP Sites U1484 (A) and U1485 (B). The first column indicates the dominant sediment texture using the same color-coding as in Figure 4A: *mud* and *silt* (green), *silty sand* (brown) and *sandy silt* (gray); the nannofossil ooze interval is highlighted in purple. Note that all three intervals dominated by *mud* and *silt* at Site U1484 correspond to coeval intervals at Site U1485, whereas the two coarser intervals with dominant *silty sand* do not. The second column shows the breakdown in percent size clay, silt and sand for both the low- and the high-resolution samples, and the third column is a plot of magnetic susceptibility at 2.5cm resolution (for Site U1485 magnetic susceptibility is from Hole A only; the gaps in the plot correspond with gaps in the core recovery). Overall, magnetic susceptibility increases at the same depths as the stratigraphic intervals dominated by coarser grained sediments (*sandy silt* and *silty sand*), whereas it is lower where *mud* and *silt* dominates including the oldest (>~370 ka) part of Site U1485. Also note how magnetic susceptibility is very similar for the last ~140kyr portion of the record at the two sites.

Figure 4: Ternary plots of the results of the LPSA analyses (%clay, %sand and %silt) following a modified version of the classification scheme of Folk (1954, 1974); the points, colored according to their age, cluster in four fields: *mud* and *silt* (green), *sandy silt* (gray) and *silty sand* (brown). A) Ternary plot for the entire dataset. Note that the majority of the samples plot in the *mud* and *silt* fields including most of the samples from the older portion of the record (>~ 300ka). B) Ternary plot with the 'high-resolution'

samples collected within or adjacent to coarser-grained beds. C) Subset of samples from B that represent the texture of sediments in the grain flows.

Figure 5: Closeups of core photographs illustrating common sediment textures. A. *Mud and silt* (U1485B-2H-2A, 1–15 cm). B. Bioturbated, nannofossil-rich *mud* with pyrite (U1485B-47H-1A, 111–125 cm). C. Homogenous *silty sand* that is part of a several meters thick massive interval interpreted as grain flow (U1485B-16H-3A, 41–55 cm). D. Homogenous *sandy silt* layer with sharp erosional base interpreted as hybrid flow (U1485A-12H-5A, 62–77 cm). E. Coquina containing large, shallow-water benthic foraminifers (U1484B-11H-4A, 35–55 cm). F. Large piece of wood (U1484B-8H-7A, 50–70 cm). G. Ash layer (U1484A-18H-4A, 115–135 cm). H. Graded *sandy silt* layer with sharp erosional base interpreted as turbidity flow (U1485A-27F-A, 40–50 cm).

Figure 6: Bivariate scattergram of mean size vs. standard deviation (SD) for samples from both IODP Sites U1484 and U1485, points are colored based on their age. The dashed line crosses the X-axis at mean size values of ~15 μm. The line separates two opposing linear trends: negative (left) and positive (right). The circled regions outline sample groups characterized by having the highest sorting (lowest SD). Group I includes mostly samples from the last ~13 kyr from both sites (upper green band in Figures 3B,C). Group II includes only samples from a massive sand layer at Hole U1485B dated to between 258.6 and 262.1 ka (coarsest interval in Figure 3C).

Figure 7: Bivariate scattergrams of particle sizes vs. magnetic susceptibility (MS) (IODP Site U1485 only). Points are colored based on the sample age. A) mean size vs. MS; B) %sand vs. MS; C) %silt vs. MS; D) %clay vs. MS.

Figure 8: Bivariate scattergrams of particle sizes vs. natural gamma radiation (NGR) (IODP Site U1485 only). Points are colored based on their age. A) %clay vs. NGR; B) %clay for samples younger than 300 ka vs. MS; C) %silt vs. NGR; D) %sand vs. NGR. The samples from >~300 ka (A, B) group in a separate, high-%clay-high-NGR field in the diagram.

Figure 9: Comparison between IODP Sites U1484 and U1485 sedimentologic and physical property data and other paleoceanographic data for the last 570 ka. The light blue bands represent stratigraphic intervals that are dominated by fine grained sediments (*mud and silt*), the dark blue band is a stratigraphic interval rich in nannofossil ooze, and the gray bands mark glacial terminations. a) Mean grain size (U1485; for the low-resolution samples only); b) %clay (U1485; for the low-resolution samples only); c) Natural Gamma Radiation (NGR) for Site U1485; d) Magnetic Susceptibility (MS) for Site U1485; e) Magnetic Susceptibility (MS) for Site U1484; f) Composite Asian Monsoon  $\delta^{18}$ O record from Sanbao Cave, China (Cheng et al., 2012 and 2016). Lower  $\delta^{18}$ O implies higher monsoon rainfall in the cave region and less monsoon rainfall in the PNG region; g) Global sea level variability (Spratt and Lisiecki, 2016).

Figure 10: Closeups of core photographs and frequency plots of the particle size analyses illustrating the main types of sedimentary structures identified in the mass gravity flow deposits. The dashed lines represent the particle size limits for clay and silt size, 4  $\mu$ m and 63  $\mu$ m, respectively. A) Example of homogenous *sandy silt* bed (U1485A-9H-7A, 55–60 cm) with sharp bottom contact, flame-like structures, and faint lamination towards the top; this bed (~125 ka) is one of the few occurrences of coarser grained *sandy silt* deposits during MIS 5e, which is otherwise dominated by *mud and silt*. B) Example of *sandy silt* bed (U1485A-5H-3A, 127–135 cm) showing evidence of a slight grain size increase towards the center of the bed (note the different scales of the vertical axis of the frequency plots). Note the preferential accumulation of coquina at the top of the bed; C) Normally graded *sandy silt* bed showing sharp bottom and bioturbated top (U1485B-8H-4A, 81–88 cm). The coarser grains at the bottom (mean = 52  $\mu$ m) also include shell fragments, whereas the fine-grained top (mean = 21  $\mu$ m) includes brown organic matter.

Figure 11) Conceptual model illustrating the evolution of the northwestern continental margin of Papua New Guinea and the Sepik Basin/Valley since the middle Pleistocene. Left: simplified lithostratigraphic column for IODP Expedition 363 Site U1485 (black = *mud* and *silt*; white

= sandy silt; grey = silty sand) and sea level variability (see Figures 3 and 10 for more details). Right: west-east oriented cross-sectional sketches that extend from the foothills of the New Guinea Highlands to the Sepik Basin/Valley, the coastal ranges (Bewani-Torricelli-Alexander Ranges), the continental margin, a margin-parallel depression and an offshore basement high that presently emerges only ~80 Km to the southeast in the island of Kairiru. The black bifurcated arrows symbolize the extent of dispersal and settlement from river plumes, the squiggly arrows the fallout of mixed, hemipelagic and pelagic sediments, the black triangles show the position of the Sepik River mouth, the dashed vertical gray line the position of IODP Site U1485 and the horizontal parallel dashed lines represent glacial-interglacial sea level variability. Each of the cross-sections describes a different phase of the evolution of the system (gray horizontal arrows arrows): I) an epicontinental sea phase which corresponds to mainly pelagic and hemipelagic sedimentation at Site U1485; II) a phase characterized by the infilling of the epicontinental sea by sediments from the proto-Sepik River and the progressive constriction of the basin due to the uplift of the not yet emerged coastal ranges (gray arrows describe faulting and uplift); this phase corresponds to the concurrent sedimentation of coarser grained sediments derived from margin-parallel grain flows (arrow head pointing out of the paper) and hemipelagic sediments; III) and IV) represent the paleogeographic configuration after the coastal ranges were fully emerged and the Sepik Basin/Valley was semi-isolated and separated from the open ocean by a shallow basement high, during glacial and interglacial conditions, respectively. During glacial conditions (III), the mouth of the Sepik River moved to the shelf edge and coarser sediments were delivered directly to the continental slope. During highstands following glacial terminations (IV), the mouth of the Sepik River was displaced further onshore, the eastern Sepik region reverted to a shallow sea and deposition of fine-grained muds similar to those deposited during the epicontinental sea phase draped the continental margins. The white arrow pointing up indicates sea level high stand conditions, while the arrow pointing down and the snowflake indicate glacial low-stand conditions.

1042

1018

1019

1020

1021

1022

1023

1024

1025

1026

1027

1028

1029

1030

1031

1032

1033

1034

1035

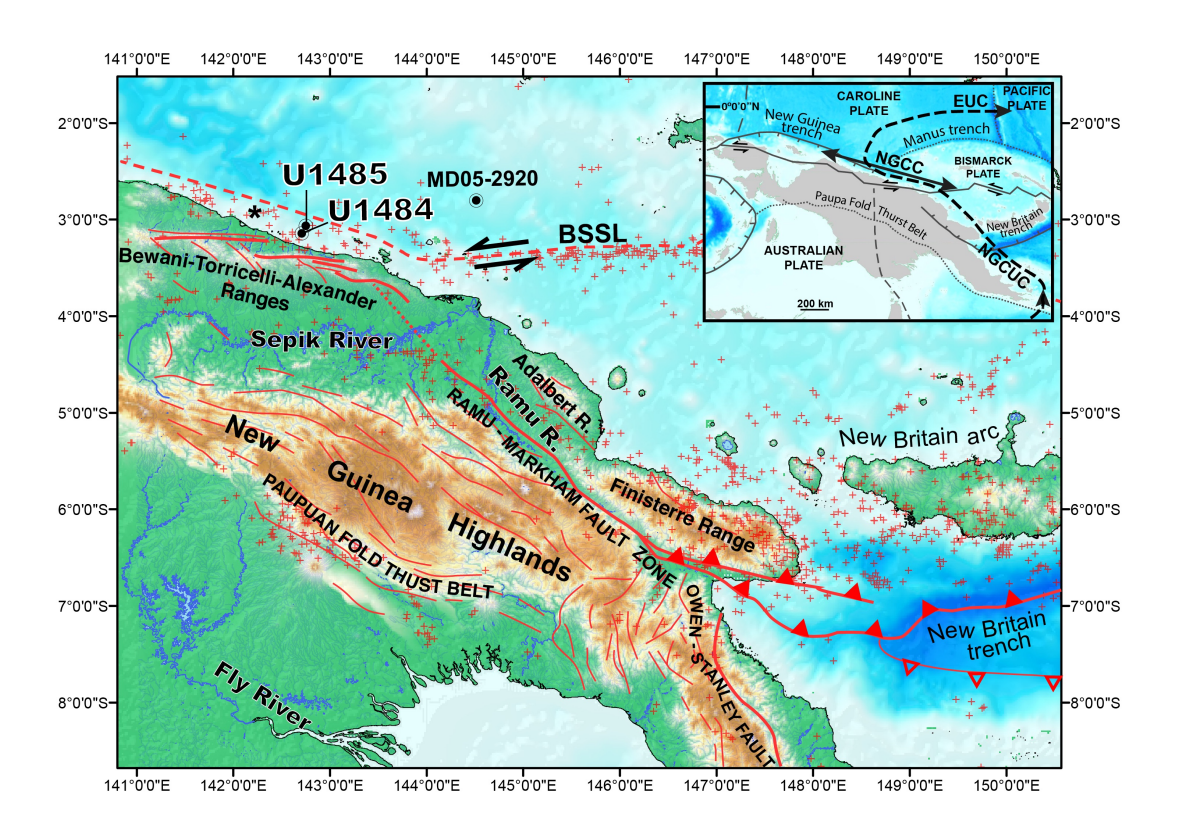
1036

1037

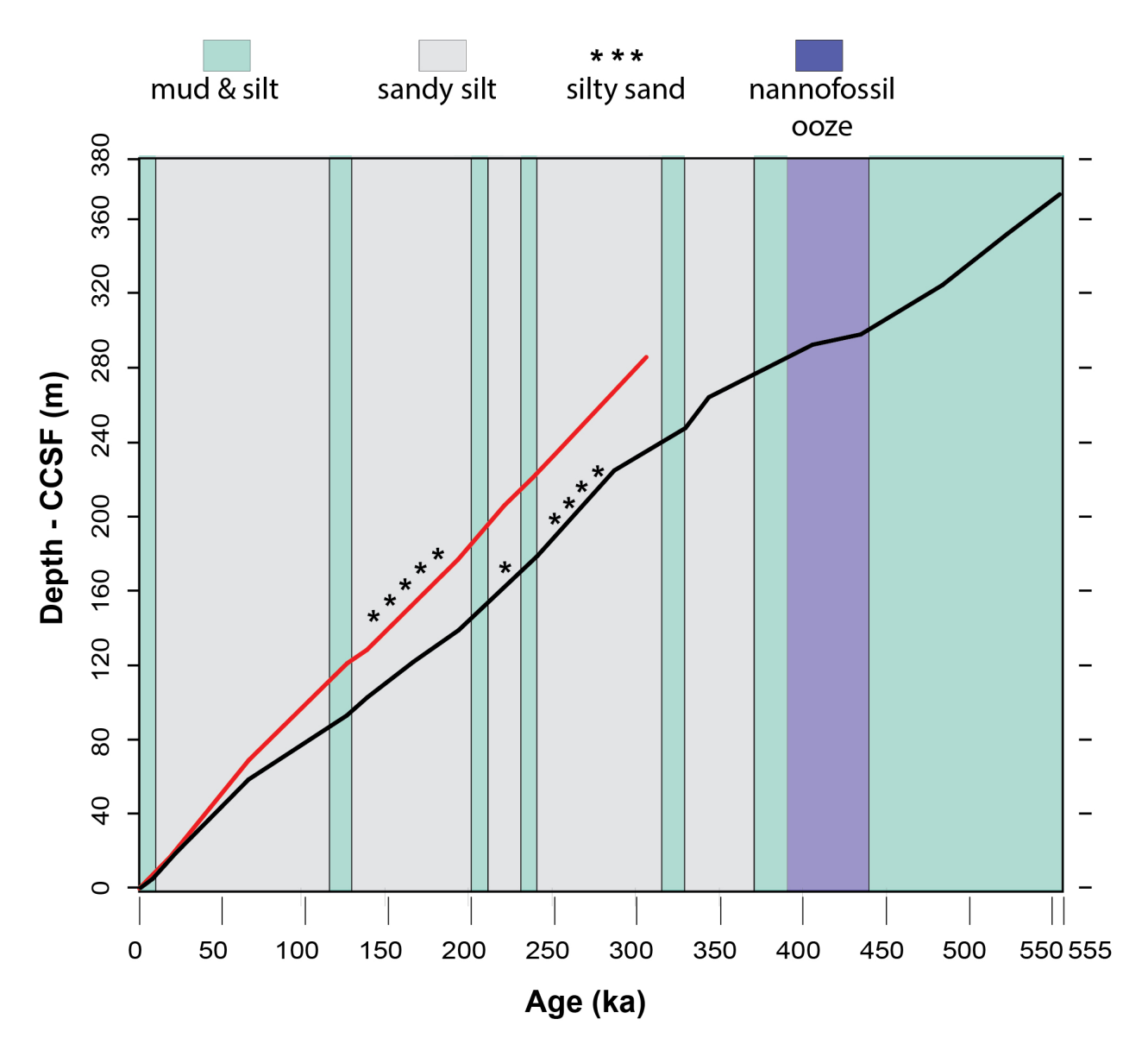
1038

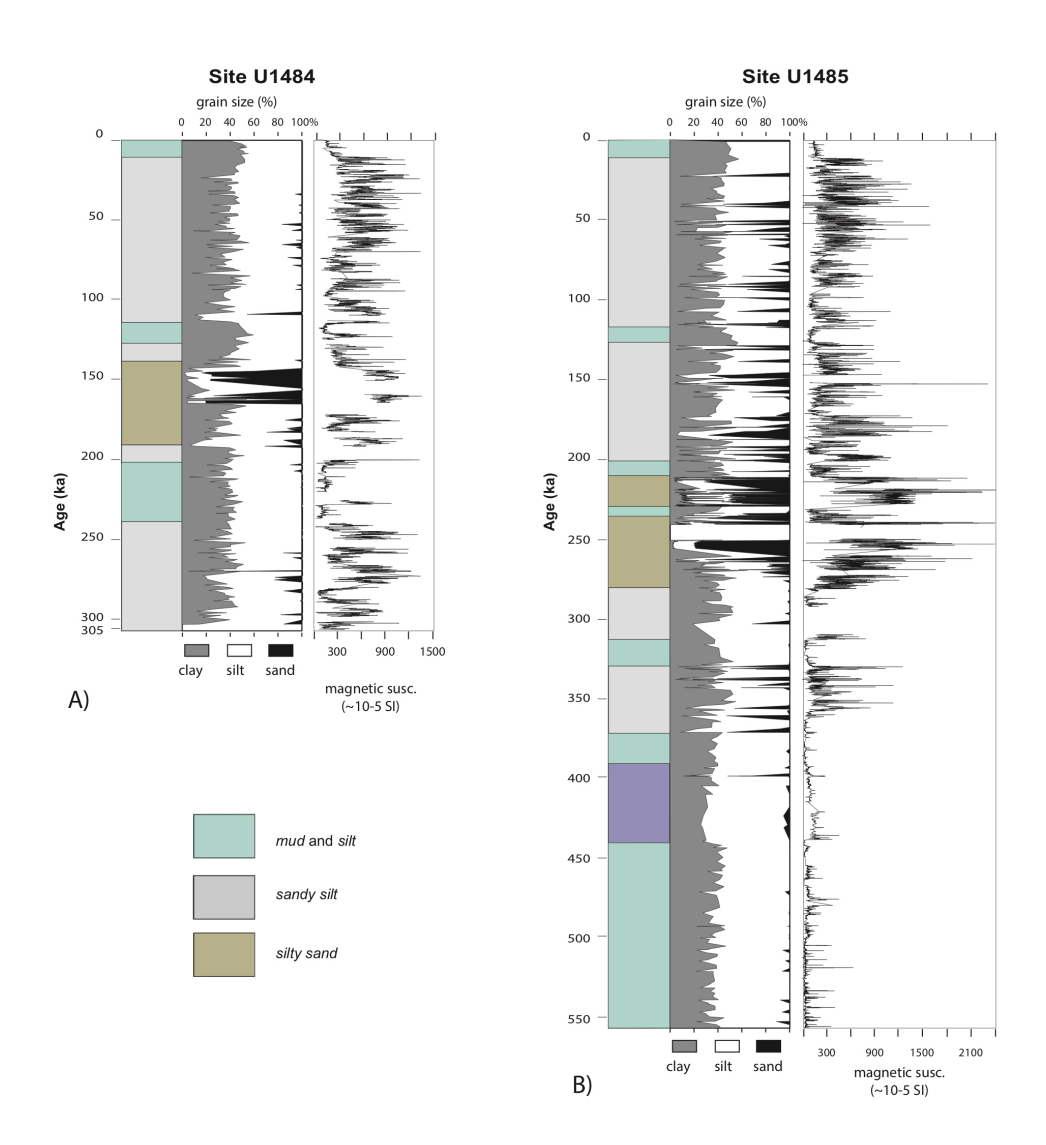
1039

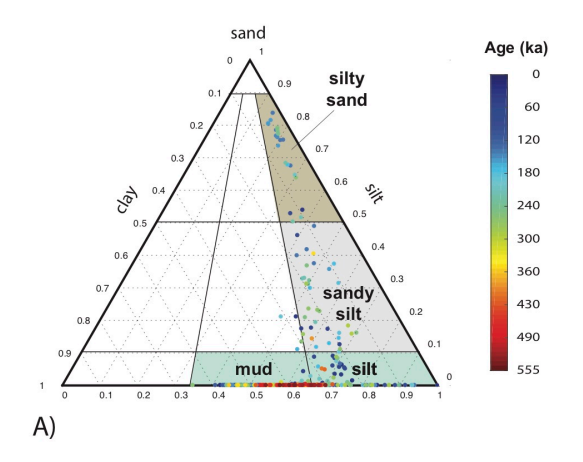
1040

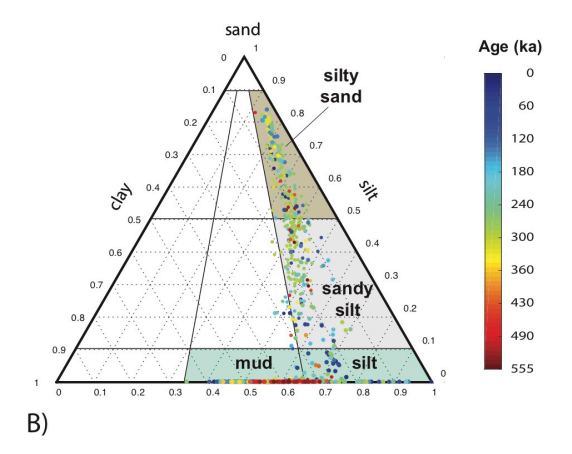


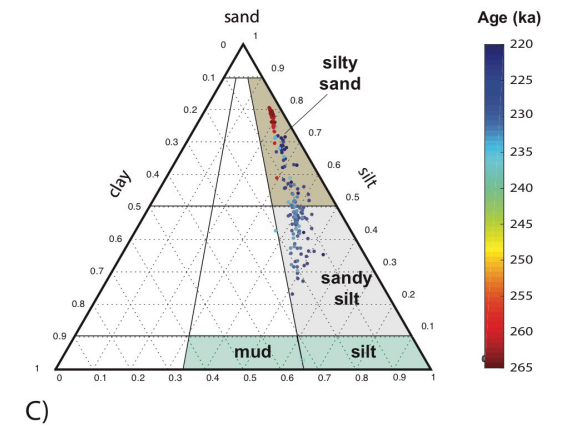
1044 Figure 1











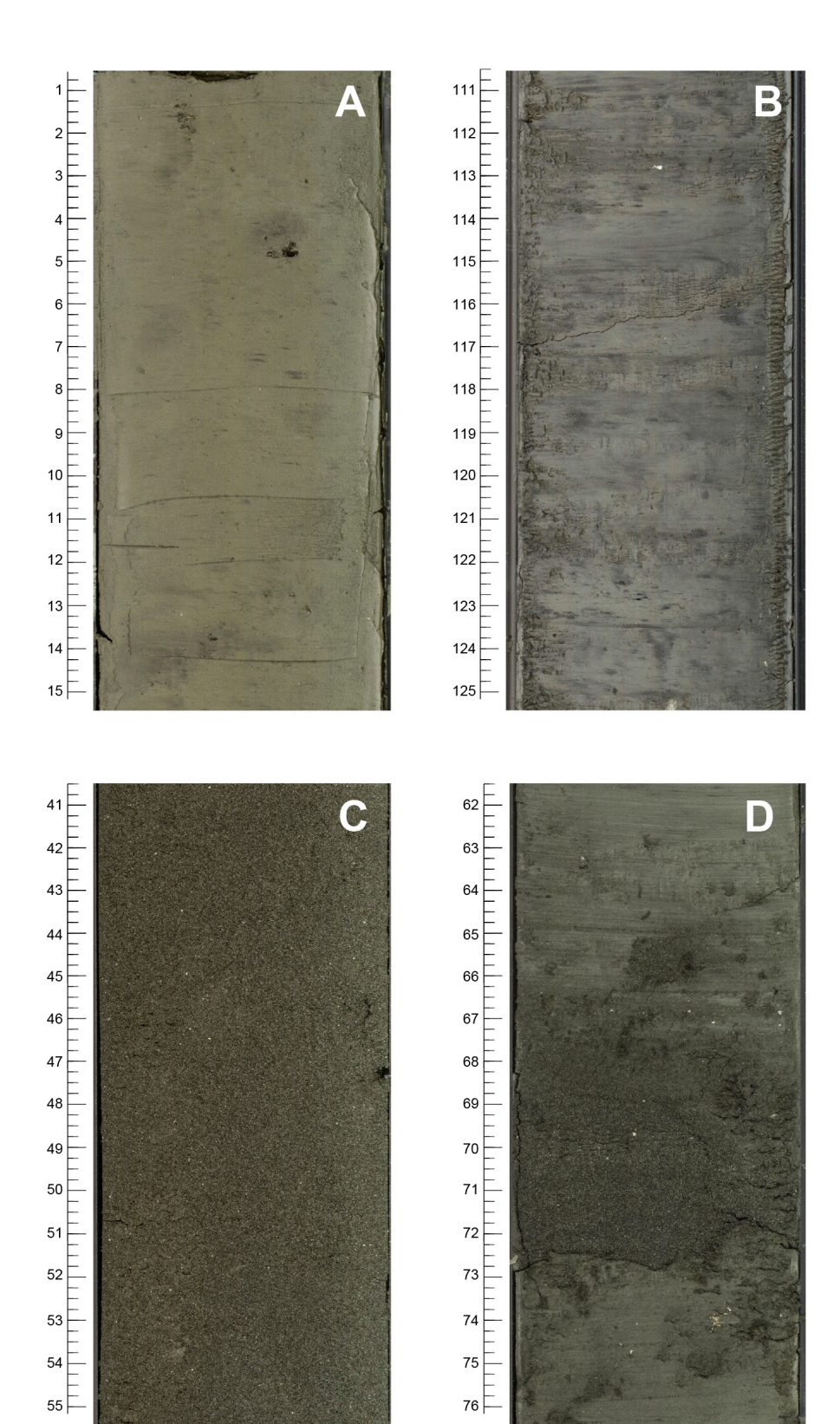
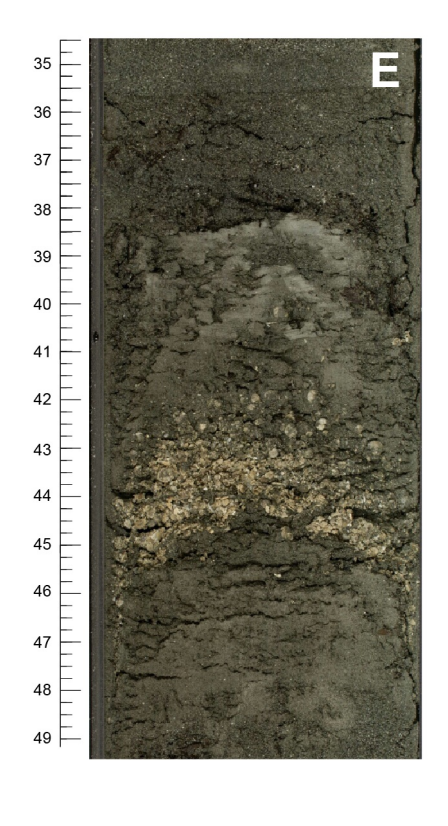
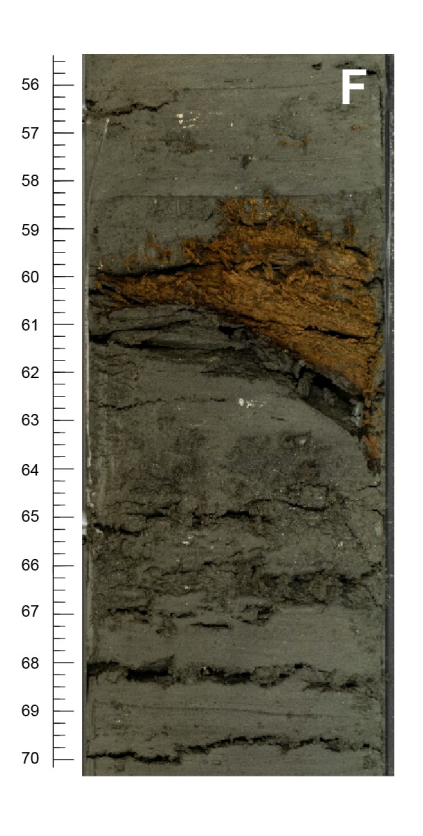


Figure 5A-D







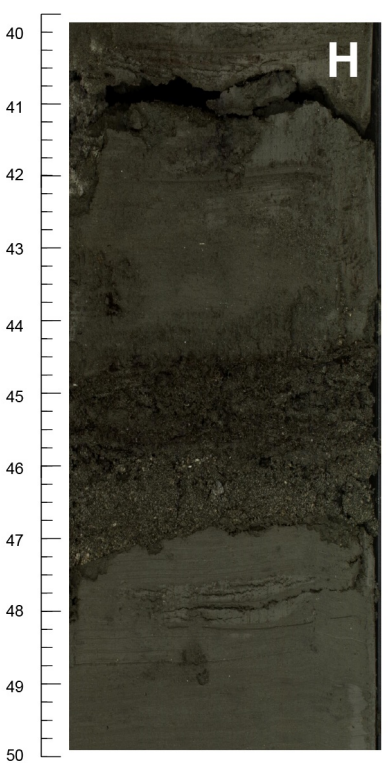
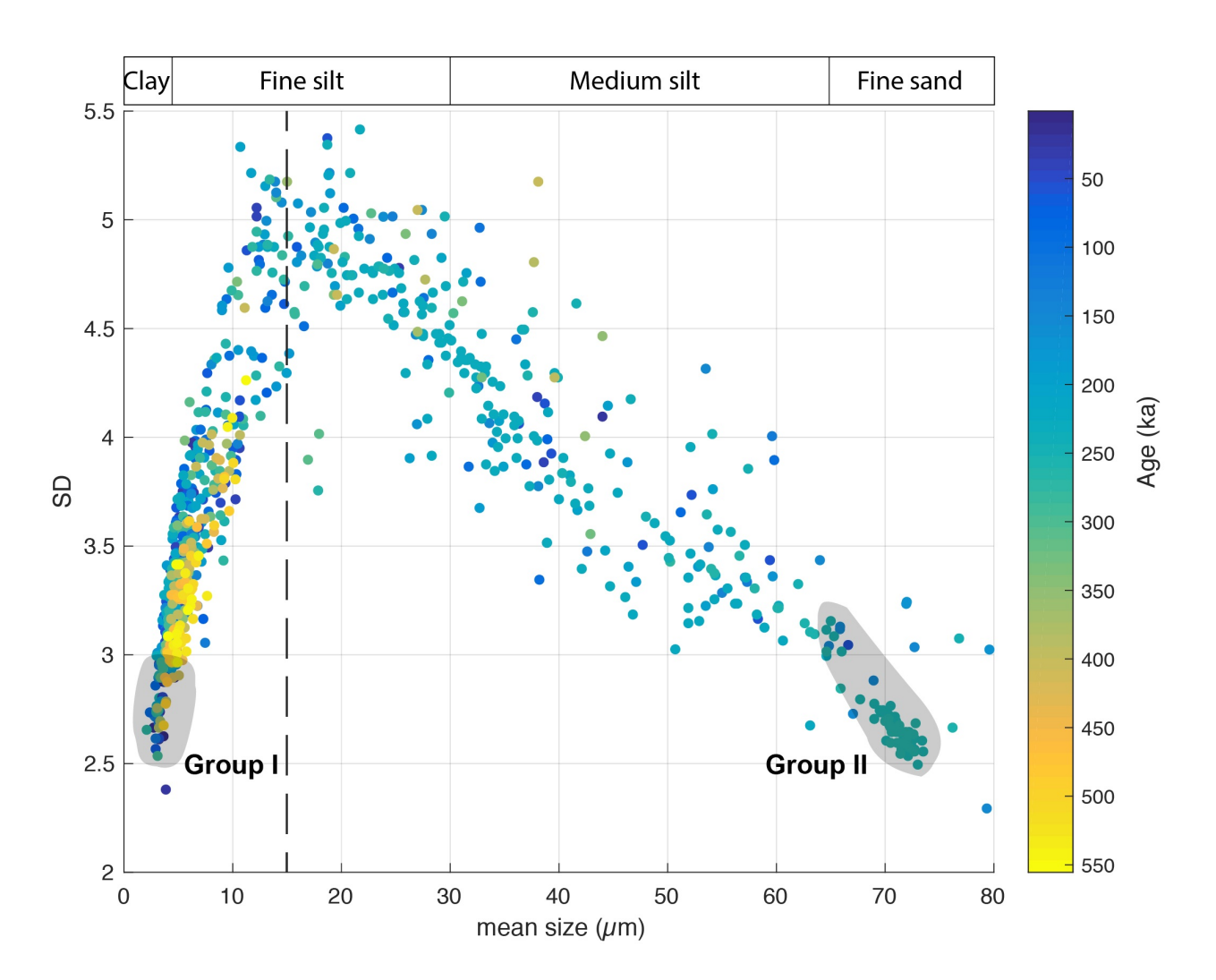


Figure E-H



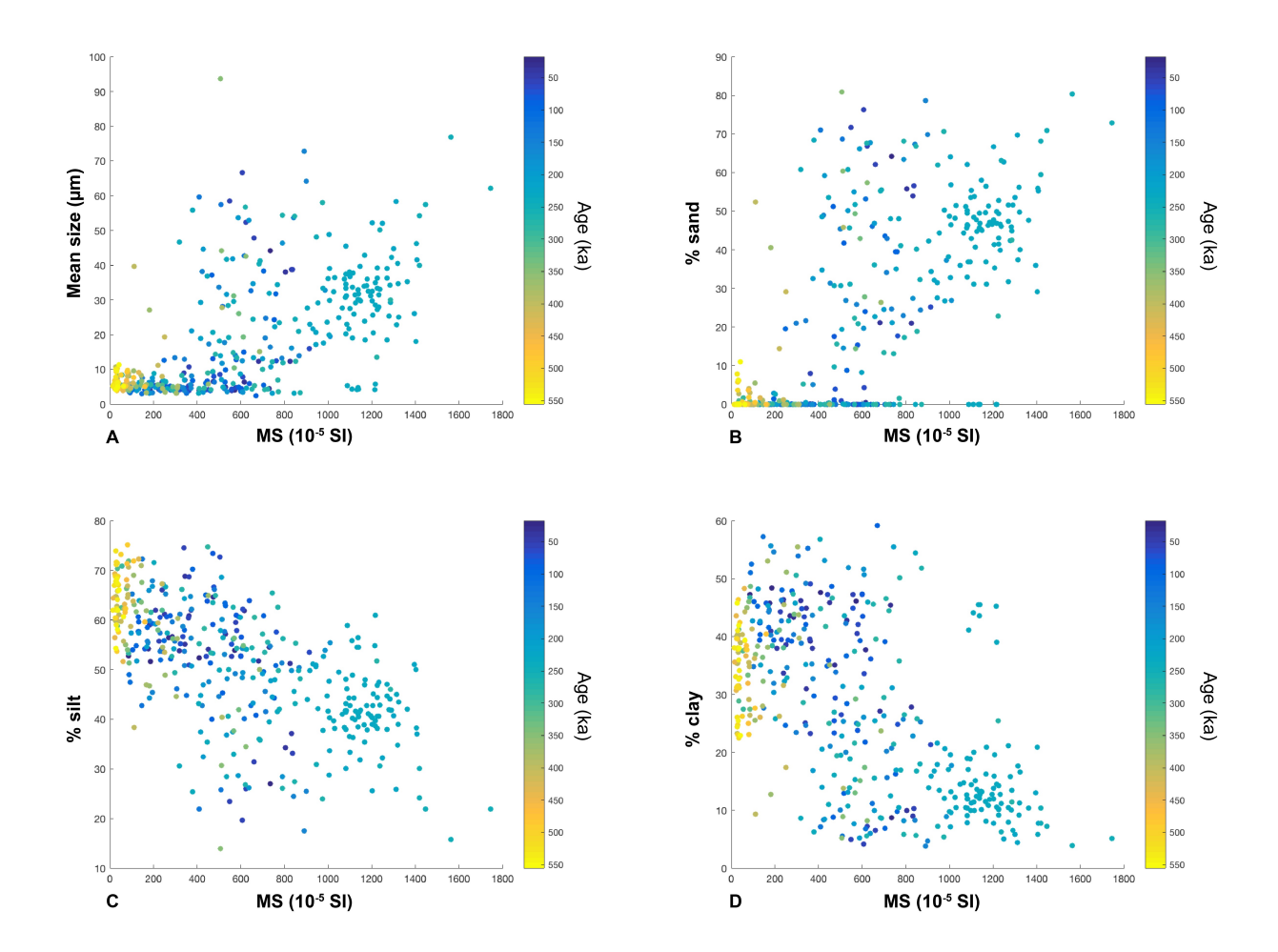
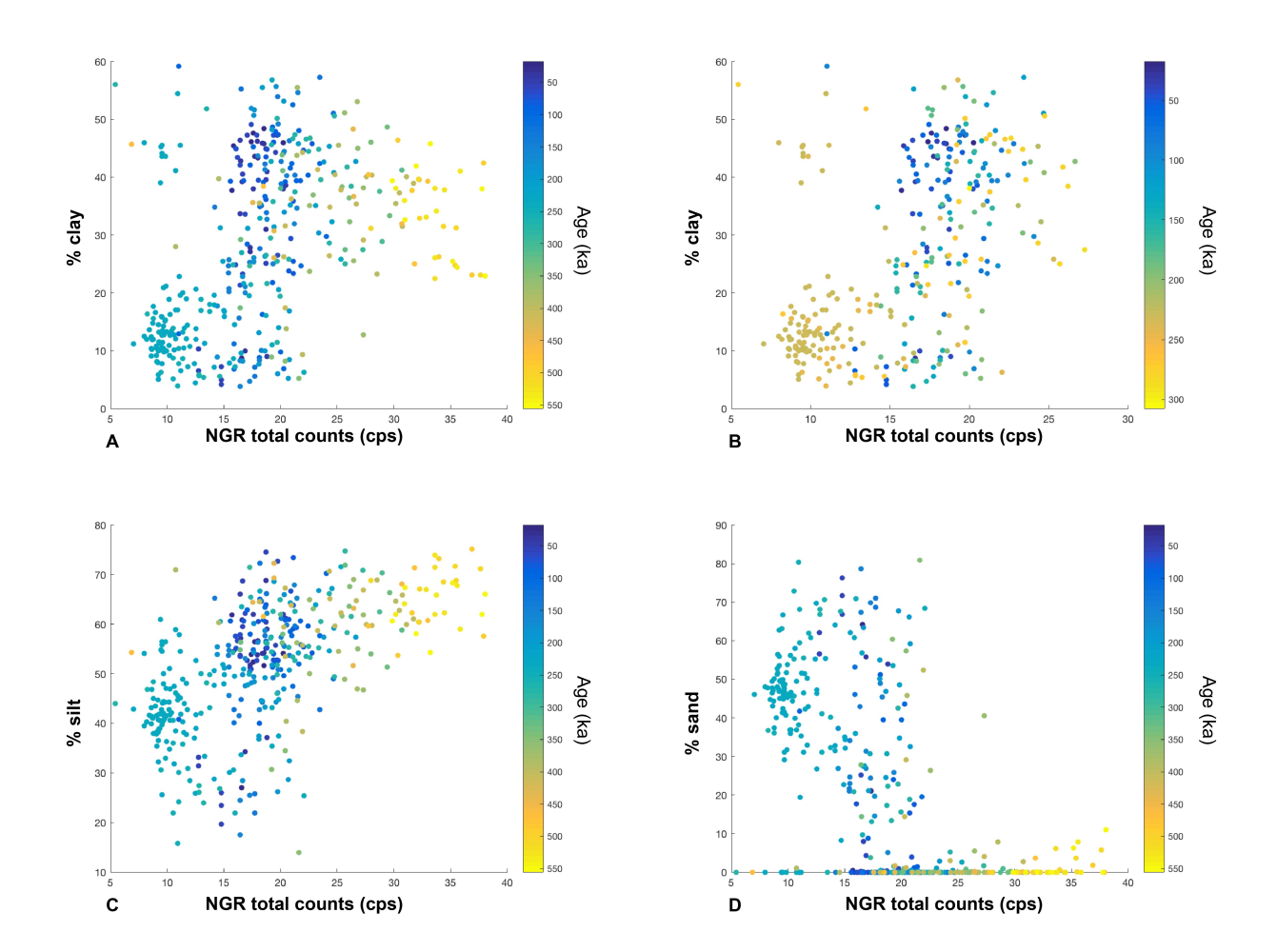
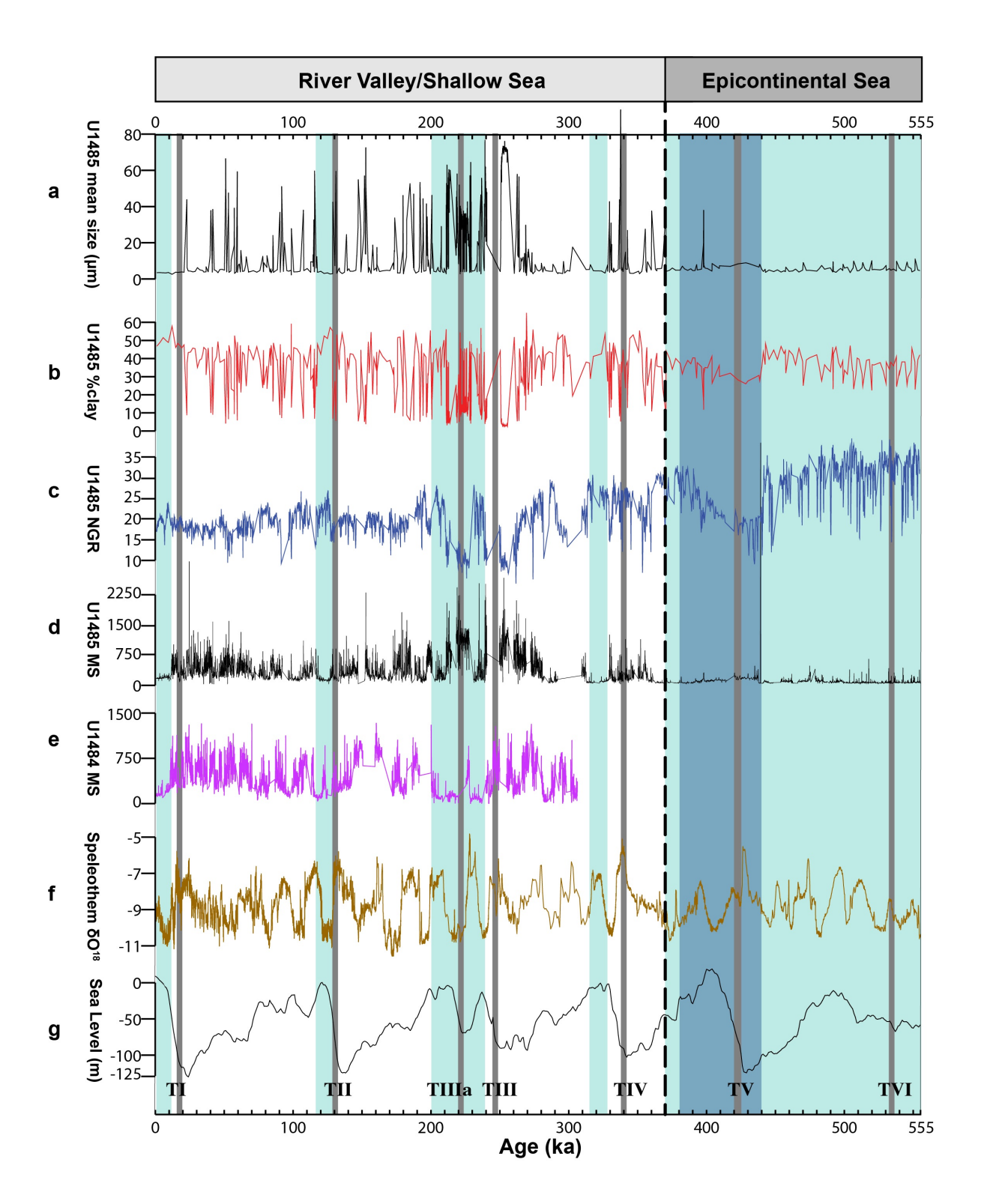
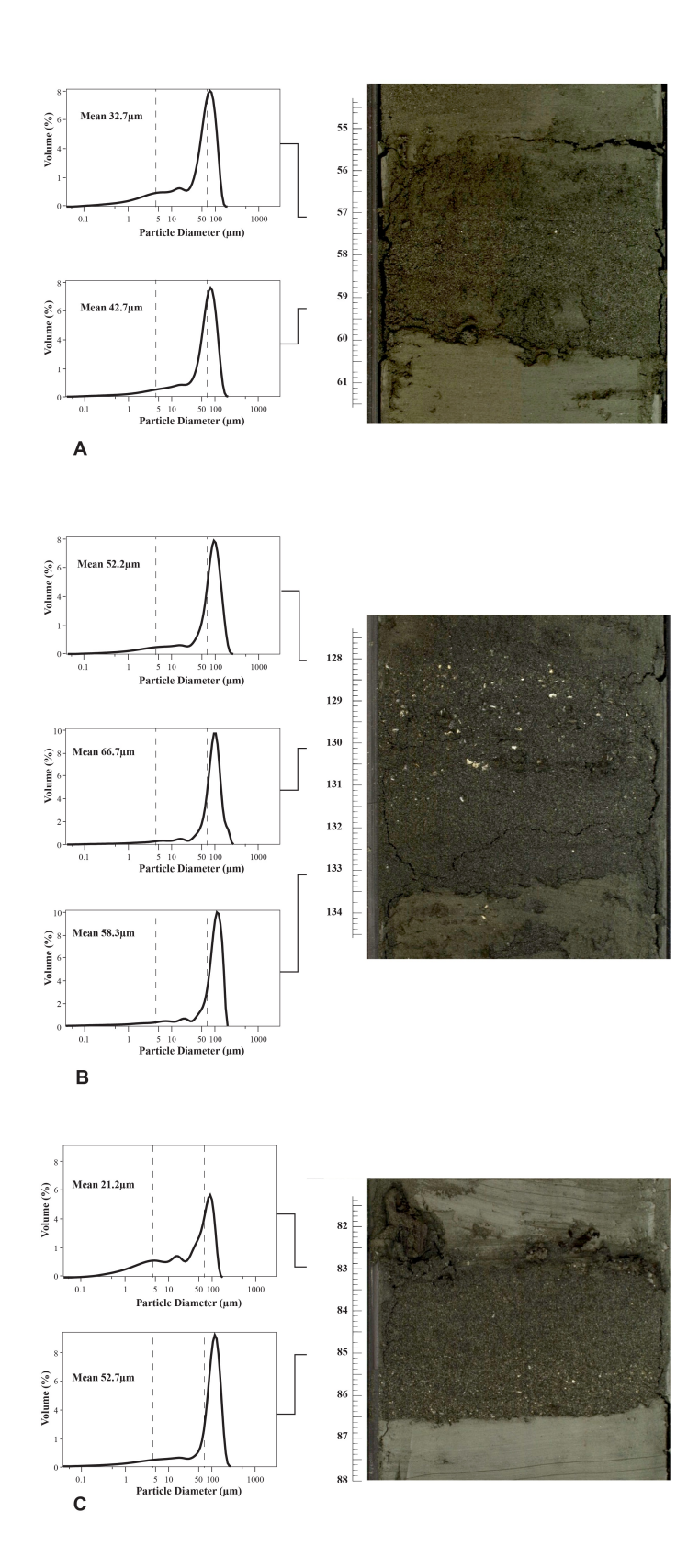


Figure 7

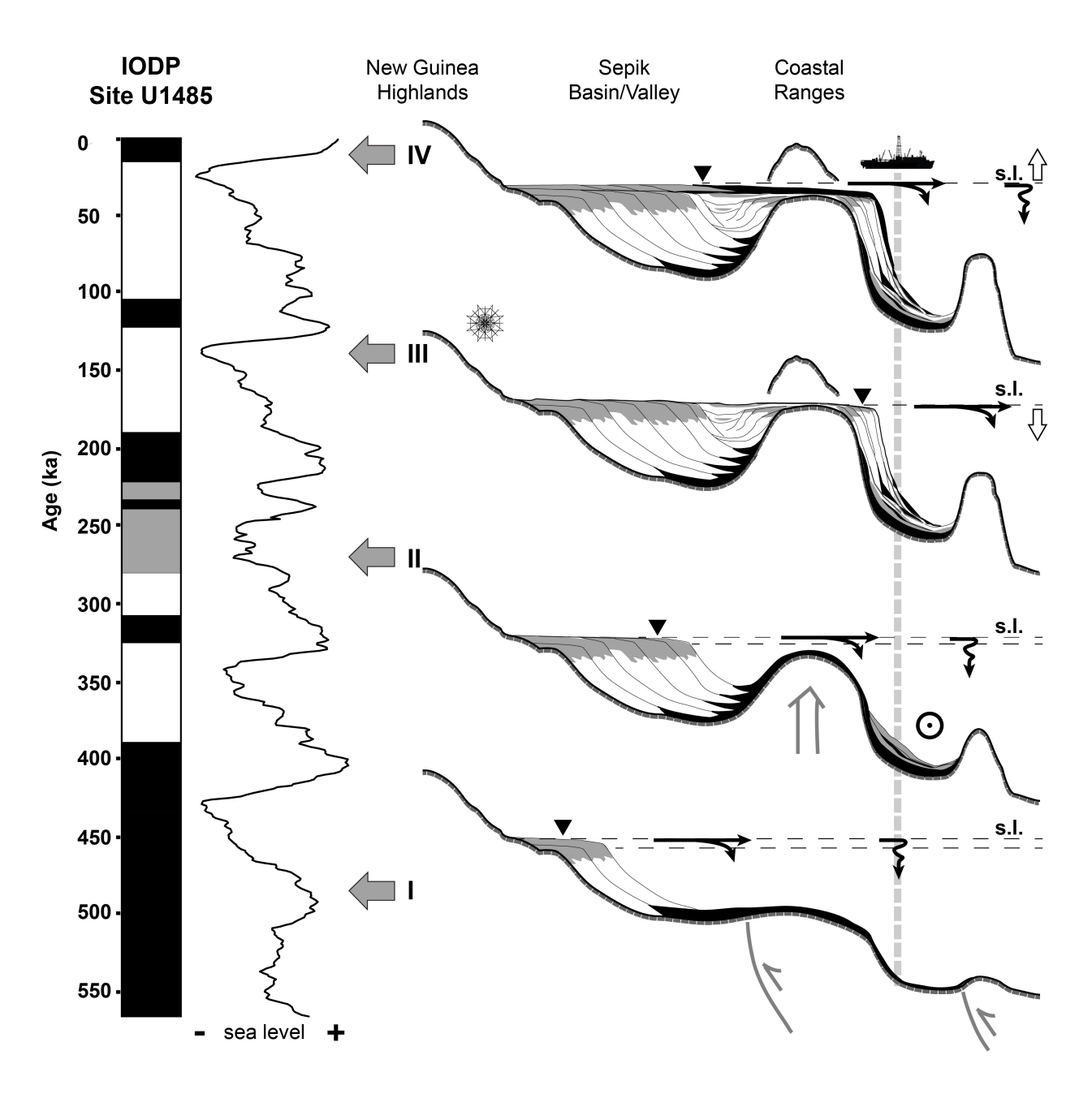


1065 Figure 8





1070 Figure 10



1072 Figure 11

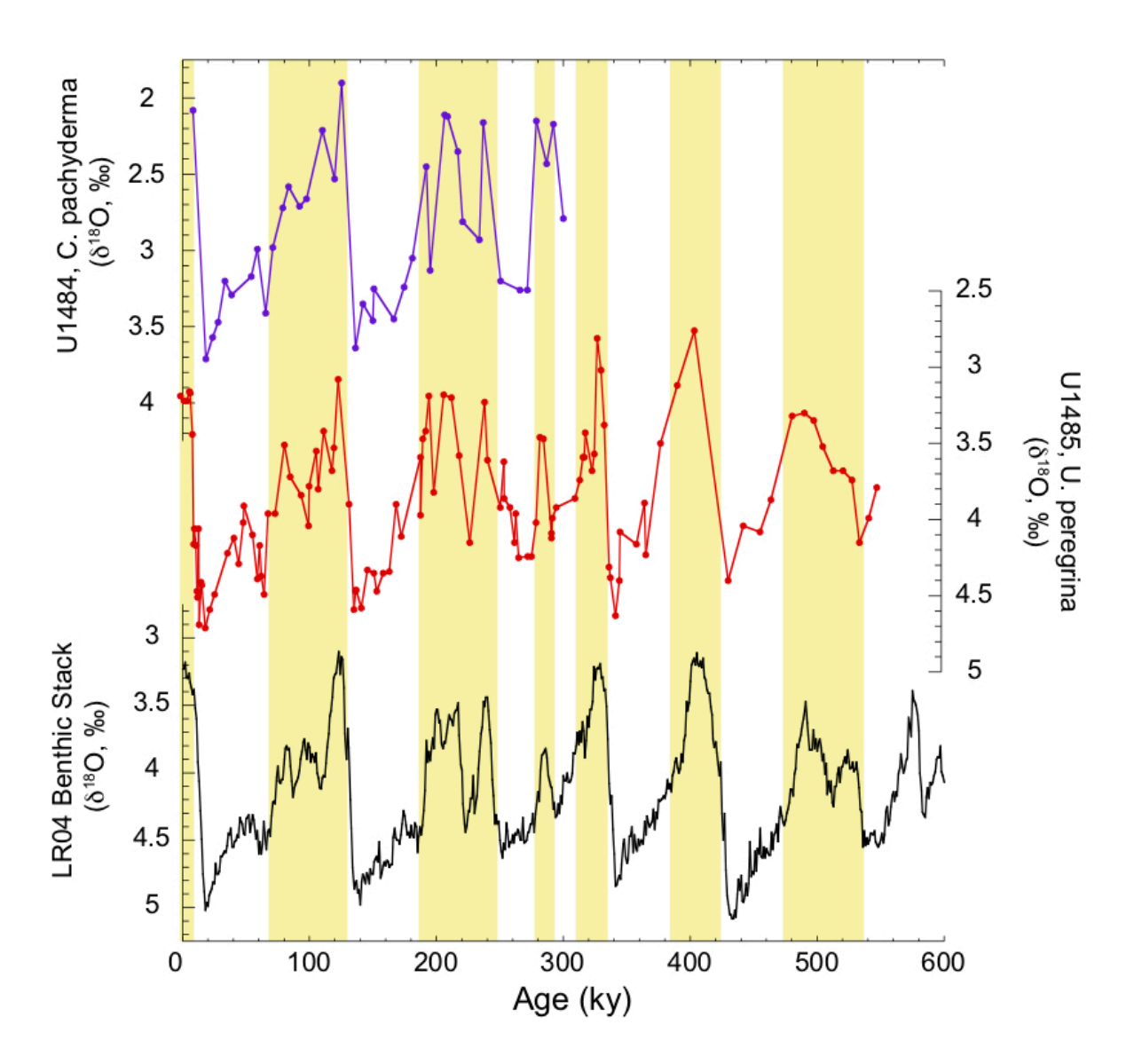


Figure S1

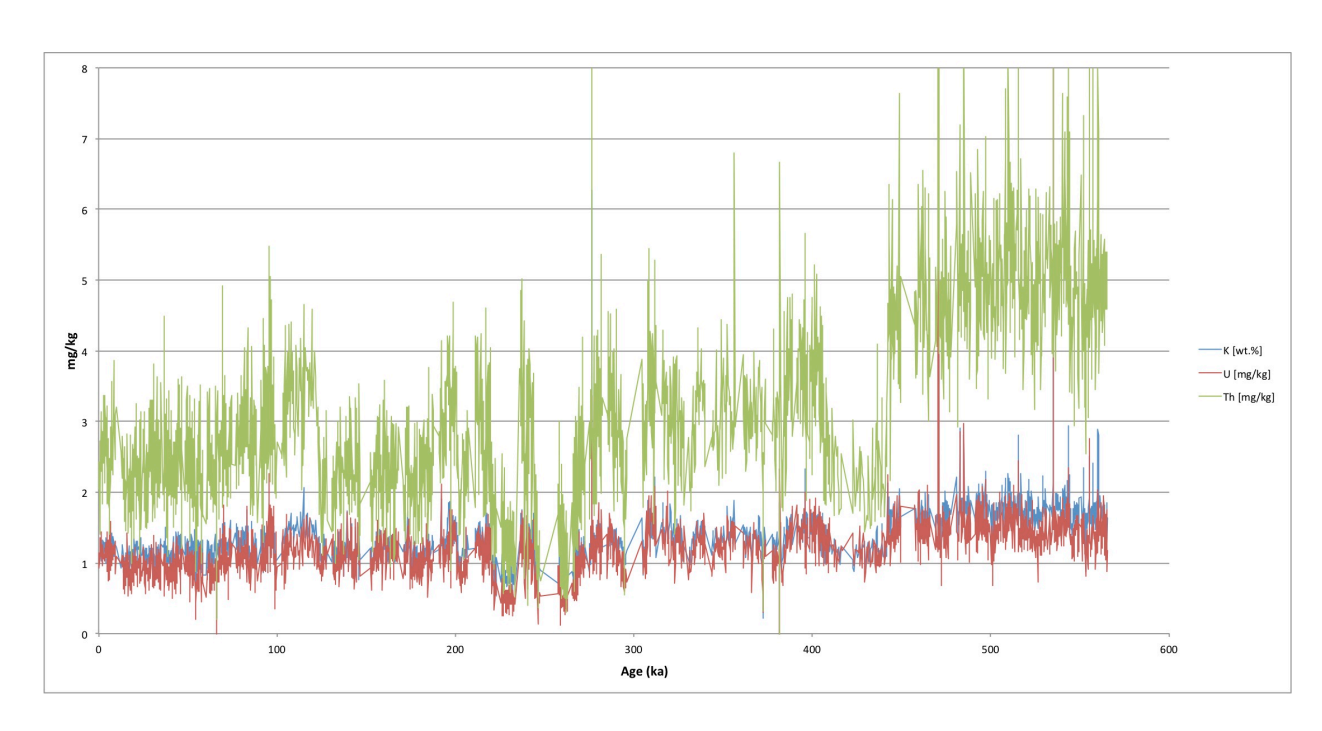


Figure S2

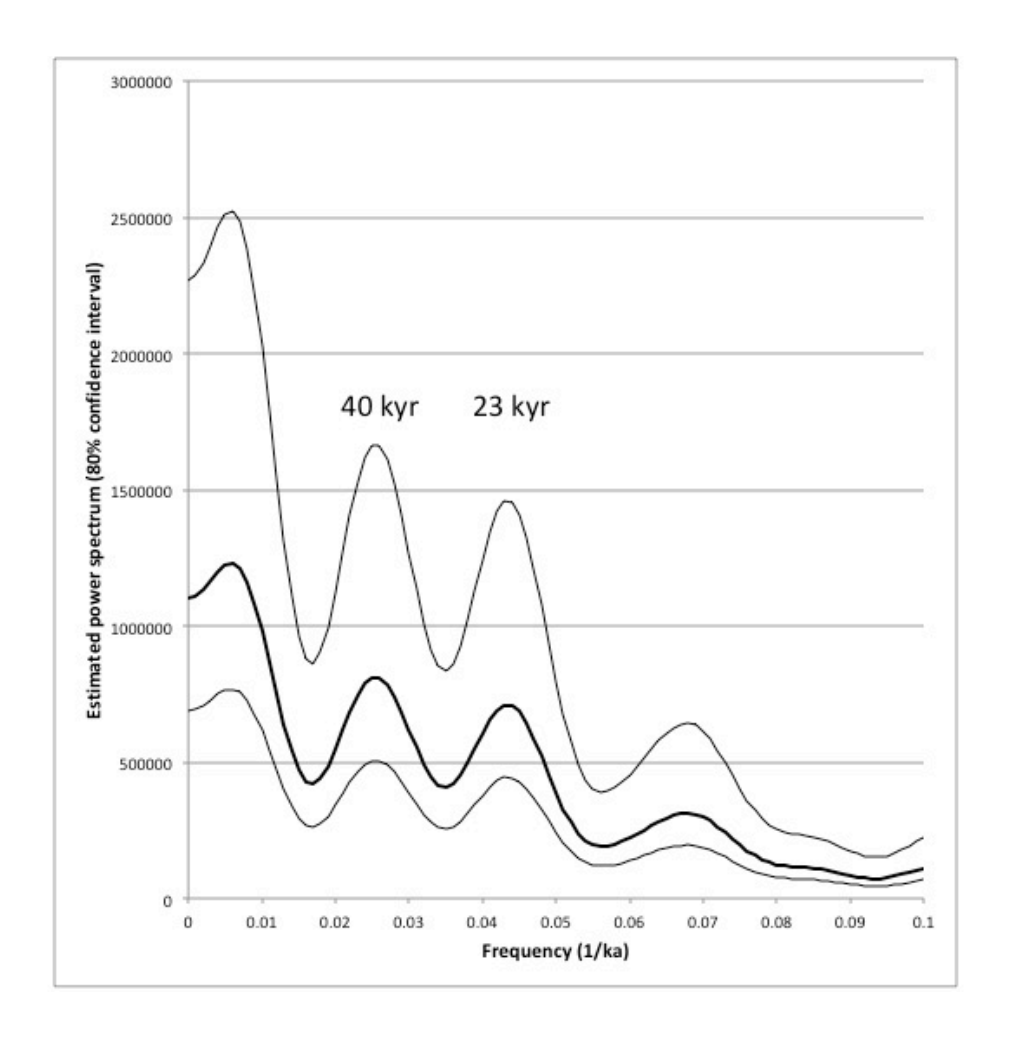


Figure S3A

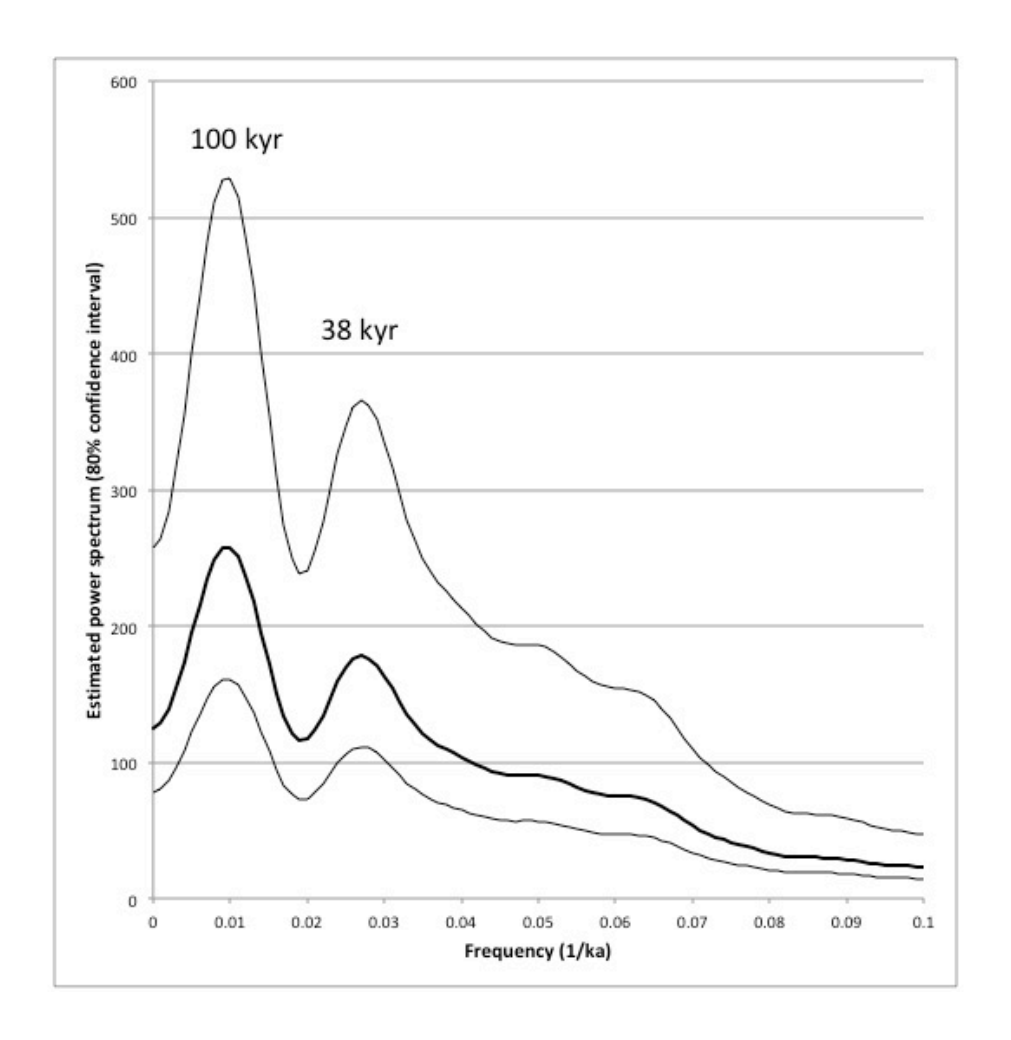


Figure S3B